Article

Cell Reports

# Human Pluripotent Stem-Cell-Derived Cortical Neurons Integrate Functionally into the Lesioned Adult Murine Visual Cortex in an Area-Specific Way

## Graphical Abstract

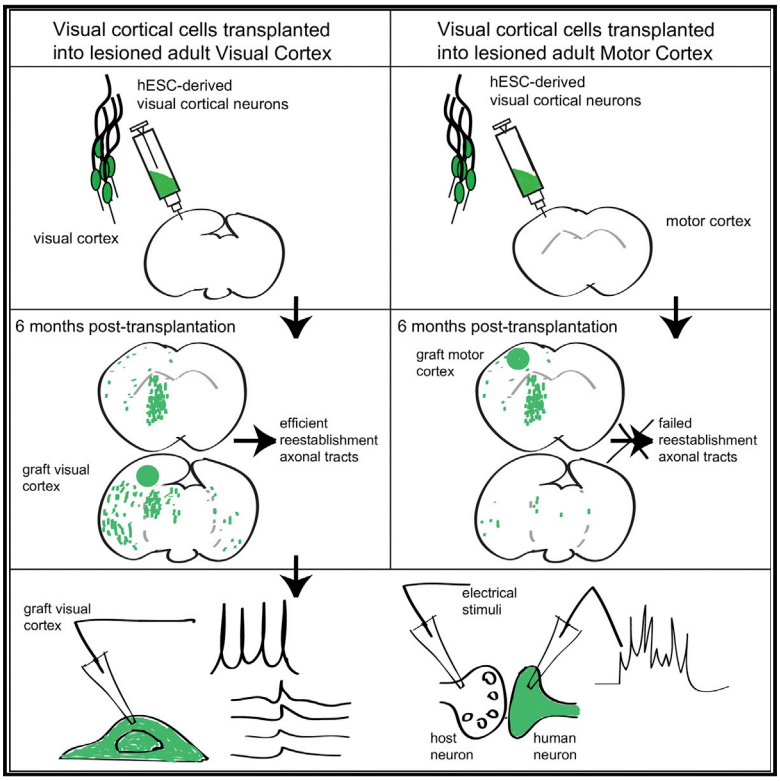


## Highlights

- Human PSC-derived cortical neurons efficiently integrate into the adult mouse brain
- PSC-derived human neurons reestablish axonal pathways in the lesioned adult cortex
- Restoration of cortical pathways requires a donor and recipient area-identity match

## Authors

Ira Espuny-Camacho, Kimmo A. Michelsen, Daniele Linaro, ..., Michele Giugliano, Afsaneh Gaillard, Pierre Vanderhaeghen

## Correspondence

pierre.vanderhaeghen@kuleuven.vib.be

## In Brief

Espuny-Camacho et al. show that transplanted ESC-derived human cortical neurons integrate functionally into the lesioned adult mouse brain. Transplanted neurons display visual cortical identity and show specific restoration of damaged cortical pathways following transplantation into the visual but not the motor cortex, suggesting the importance of areal-identity match for successful cortical repair.

Espuny-Camacho et al., 2018, Cell Reports *23*, 2732–2743
May 29, 2018 
https://doi.org/10.1016/j.celrep.2018.04.094

CellPress

OPEN ACCESS
CellPress

Cell Reports
Article

# Human Pluripotent Stem-Cell-Derived Cortical Neurons Integrate Functionally into the Lesioned Adult Murine Visual Cortex in an Area-Specific Way

Ira Espuny-Camacho,[1,2,3,4,5] Kimmo A. Michelsen,[1] Daniele Linaro,[1,2,3,6] Angéline Bilheu,[1] Sandra Acosta-Verdugo,[1,11] Adèle Herpoel,[1] Michele Giugliano,[6,7,8] Afsaneh Gaillard,[9] and Pierre Vanderhaeghen[1,2,3,10,12,*]

[1]Université Libre de Bruxelles (ULB), Institut de Recherches en Biologie Humaine et Moléculaire (IRIBHM), and ULB Neuroscience Institute (UNI), 1070 Brussels, Belgium
[2]VIB-KU Leuven Center for Brain & Disease Research, 3000 Leuven, Belgium
[3]Department of Neurosciences, Leuven Brain Institute, KU Leuven, 3000 Leuven, Belgium
[4]Laboratory of Stem Cell Biology and Pharmacology of Neurodegenerative Diseases, Department of Biosciences, Università degli Studi di Milano, Via Francesco Sforza 35, 20122 Milano, Italy
[5]INGM Foundation, Via Francesco Sforza 35, 20122 Milano, Italy
[6]Theoretical Neurobiology and Neuroengineering Laboratory, Department of Biomedical Sciences, University of Antwerp, 2610 Wilrijk, Belgium
[7]Department of Computer Science, University of Sheffield, S1 4DP Sheffield, UK
[8]Laboratory of Neural Microcircuitry, Brain Mind Institute, EPFL, 1015 Lausanne, Switzerland
[9]INSERM U-1084, Experimental and Clinical Neurosciences Laboratory, Cellular Therapies in Brain Diseases Group, University of Poitiers, 86022 Poitiers, France
[10]WELBIO, ULB, Brussels, Belgium
[11]Present address: Feinberg Cardiovascular Research Institute, Northwestern University, Chicago, IL 60611, USA
[12]Lead Contact
*Correspondence: pierre.vanderhaeghen@kuleuven.vib.be
https://doi.org/10.1016/j.celrep.2018.04.094

## SUMMARY

**The transplantation of pluripotent stem-cell-derived neurons constitutes a promising avenue for the treatment of several brain diseases. However, their potential for the repair of the cerebral cortex remains unclear, given its complexity and neuronal diversity. Here, we show that human visual cortical cells differentiated from embryonic stem cells can be transplanted and can integrate successfully into the lesioned mouse adult visual cortex. The transplanted human neurons expressed the appropriate repertoire of markers of six cortical layers, projected axons to specific visual cortical targets, and were synaptically active within the adult brain. Moreover, transplant maturation and integration were much less efficient following transplantation into the lesioned motor cortex, as previously observed for transplanted mouse cortical neurons. These data constitute an important milestone for the potential use of human PSC-derived cortical cells for the reassembly of cortical circuits and emphasize the importance of cortical areal identity for successful transplantation.**

## INTRODUCTION

Neurodegenerative diseases, brain injury, and stroke are major causes of neuronal cell loss in the adult brain. Together with *in vivo* reprogramming (Arlotta and Berninger, 2014; Gascón et al., 2017), transplantation of neural cells is a promising avenue for the replacement of lost neurons and damaged neural circuits (Barker et al., 2015; Gage and Temple, 2013; Goldman, 2016; Tabar and Studer, 2014). An ideal cell transplant approach should lead to the replacement of the lost neuronal subtypes and neural circuits in a comprehensive and specific way. Compared, for instance, with the replacement of substantia nigra neurons in Parkinson disease, this seems to be particularly challenging for the cerebral cortex, both conceptually and technically, given its unparalleled neuronal diversity, complex connectivity, and function. However, several independent studies have demonstrated the potential of transplanted mouse cortical cells, whether derived from mouse embryonic tissue or embryonic stem cells, for the replacement of lost neurons following a cortical lesion in the adult mouse (Falkner et al., 2016; Gaillard et al., 2007; Michelsen et al., 2015; Péron et al., 2017). Such transplanted cells display specific patterns of synaptic inputs, making them function in a highly similar way to endogenous neurons (Falkner et al., 2016). They also present surprisingly high levels of specificity in terms of cortex areal identity. For instance, replacement of lesioned motor cortex with embryonic motor cortex tissue (Gaillard et al., 2007) can lead to the selective re-establishment of motor axonal pathways, but the use of transplants derived from the visual cortex does not lead to any efficient repair. Similarly, the transplantation of mouse visual cortex-like cells derived from embryonic stem cells (ESCs) (Gaspard et al., 2008) can lead to the efficient replacement of lesioned axonal pathways of the visual cortex but not the motor cortex (Michelsen et al., 2015). Thus, successful transplantation in these cases

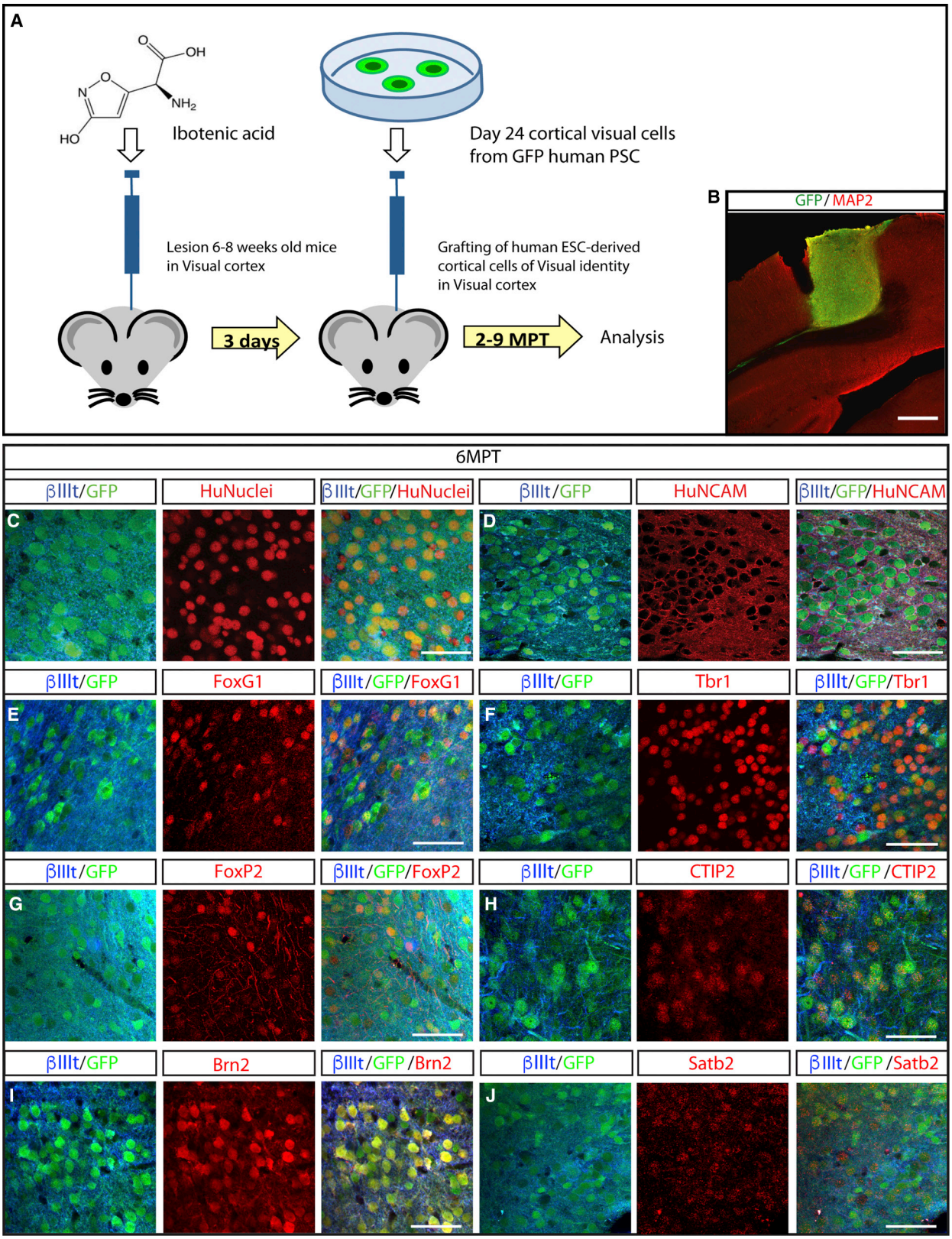


*(legend on next page)*

was achieved only if there was a match between the areal identity (frontal versus occipital) of the lesioned and the transplanted cortical cells (Michelsen et al., 2015).

From a translational viewpoint, the ability of human pluripotent stem cells (PSCs) to contribute to the repair of cortical lesions is of paramount importance, given the limited availability of fetal material. We and others have shown that human ESCs and induced PSCs (iPSC) can be differentiated into pyramidal glutamatergic cortical neurons from all cortical layers (van den Ameele et al., 2014; Eiraku et al., 2008; Espuny-Camacho et al., 2013; Shi et al., 2012). The default differentiation of human ESCs and iPSCs cultured in the absence of any morphogens but in the presence of Noggin for human ectoderm acquisition recapitulates several main hallmarks of *in vivo* corticogenesis, such as temporal patterning *in vitro* (Espuny-Camacho et al., 2013). Moreover, upon transplantation into newborn recipient mice, the cortical neurons send specific patterns of cortical axonal projections at far distances from the graft location and are integrated in mouse neuronal networks (Espuny-Camacho et al., 2013).

Human ESC-derived neurons were recently shown to establish functional synapses following transplantation into damaged cortical areas in the adult mouse (Tornero et al., 2013, 2017), but the specificity of the cortical fate of the transplanted cells and of their axonal input/output remains to be explored. Here, we investigated whether and how human ESC-derived cortical neurons corresponding mostly to a visual-like identity (Espuny-Camacho et al., 2013) transplanted into the lesioned adult murine cortex could integrate into the lesioned area and participate in the reassembly of cortical circuits. We found that the human neurons transplanted into the lesioned cortex acquire the molecular and axonal projection characteristics of all six cortical layers, while displaying a high degree of visual areal specificity. They also display features of functional neurons in terms of synaptic connectivity. The success of transplantation is highly dependent on a match of (visual) areal identity between the lesioned and the transplanted neurons. These results imply that human ESC-derived cortical neurons also can efficiently differentiate and establish cortical-specific neural connections in the less permissive environment of the adult lesioned brain.

## RESULTS

### Human PSC-Derived Cortical Neurons Integrate into the Adult Lesioned Murine Cortex following Transplantation

To determine whether transplanted human PSC-derived cortical neurons can integrate in the lesioned adult mouse cortex, we used focal cortical lesioning mediated by injection of neurotoxic ibotenic acid, as used for the transplantation of mouse ESC-derived cortical neurons (Michelsen et al., 2015) (Figure 1A). Three days later, we transplanted cortical-like cells differentiated from GFP-expressing human ESCs (Espuny-Camacho et al., 2013) into the same lesioned area. This *in vitro* corticogenesis model generates human neurons from all different cortical layers in a temporal manner. We showed that such human cortical cells transplanted into immunodeficient newborn mice generate neurons with a visual-like areal identity at early stages that efficiently integrate into mouse neural networks *in vivo* (Espuny-Camacho et al., 2013). We, therefore, first focused on transplantation into the lesioned visual cortex, as performed previously for mouse ESCs (Michelsen et al., 2015). Following 3 weeks of *in vitro* differentiation, GFP-expressing human ESC-derived cortical cells were dissociated and transplanted in the lesioned visual cortex of immunodeficient adult mice. The presence of the human transplants was assessed by GFP immunostainings at 1–2 and 6 months post-transplantation (MPT) and found in 11 of 21 (52%) animals that underwent transplantation. As expected, transplants were located in the cortex or in the underlying white matter (Figures 1B, 2A, S1A, S1B, S2E, and S3A). We then compared the transplants at 2 and 6 MPT for maturation and integration.

At 2 MPT, transplants were still rather immature, with the presence of neural progenitors, displayed in rosette-like structures and expressing markers of proliferation (Figures S1A, S1C, and S1E), while the expression of mature neuronal markers such as VGlut1 and NeuN remained low (Figures S1G and S1I). In contrast, at 6 MPT, the transplants, found in 58% of animals, presented a more mature pattern, with far fewer or no rosette-like structures and with few proliferative cells or progenitors (Figures S1B, S1D, and S1F). $GFP^+$-transplanted cells were positive for the human specific markers HuNuclei and human neural cell adhesion molecule (NCAM), and broadly expressed the telencephalic marker FoxG1, the neuronal marker beta 3 class III tubulin (Figures 1C–1E), and mature neuronal markers such as VGlut1, NeuN, and MAP2 (Figures S1H, S1J, and 1B). Moreover, these neurons expressed a diverse repertoire of layer-specific cortical pyramidal neuronal markers, including deep layer VI; V markers Tbr1, Foxp2, and Ctip2; and upper layer IV-II markers Satb2 and Brn2 (Figures 1F–1J and S2I–S2L), in accordance with results previously obtained with human cortical cells transplanted in neonatal cortex (Espuny-Camacho et al., 2013).

We then examined qualitatively the patterns of axonal projections of the transplants. At 2 MPT, consistent with immaturity, the transplants displayed little neurite outgrowth within the host, with $GFP^+$ axons that were still positive for immature markers such as doublecortin (DCX) (Figures S2A–S2D). Axonal processes were detected mostly close to the site of the graft in the ipsilateral cortex, with few $GFP^+$ axons extending distantly along the corpus callosum, along the internal capsule, and in the striatum (Figures S2E–S2H). In contrast, at 6 MPT, in accordance with the expression of generic and specific markers of mature pyramidal neurons from all cortical layers, the transplants displayed robust

**Figure 1. Grafted Human ESC-Derived Neurons in the Adult Murine Cortex Express Telencephalic and Cortical Layer-Specific Markers**

(A) Experimental scheme of the lesioning/transplantation experiments in the visual cortex.

(B) Immunofluorescence image showing the $GFP^+$ transplant (green) and MAP2 (red) staining of the visual cortex and the transplant.

(C–J) Immunofluorescence images showing the $GFP^+$ graft (green), beta 3 class III tubulin (blue), and the human markers HuNuclei and HuNCAM (red; C and D); the telencephalic marker FoxG1 (red; E); and the cortical layer markers Tbr1 (F), Foxp2 (G), CTIP2 (H), Brn2 (I), Satb2 (J) (red) at 6 MPT.

Scale bars: 500 μm (B), 50 μm (C–J).

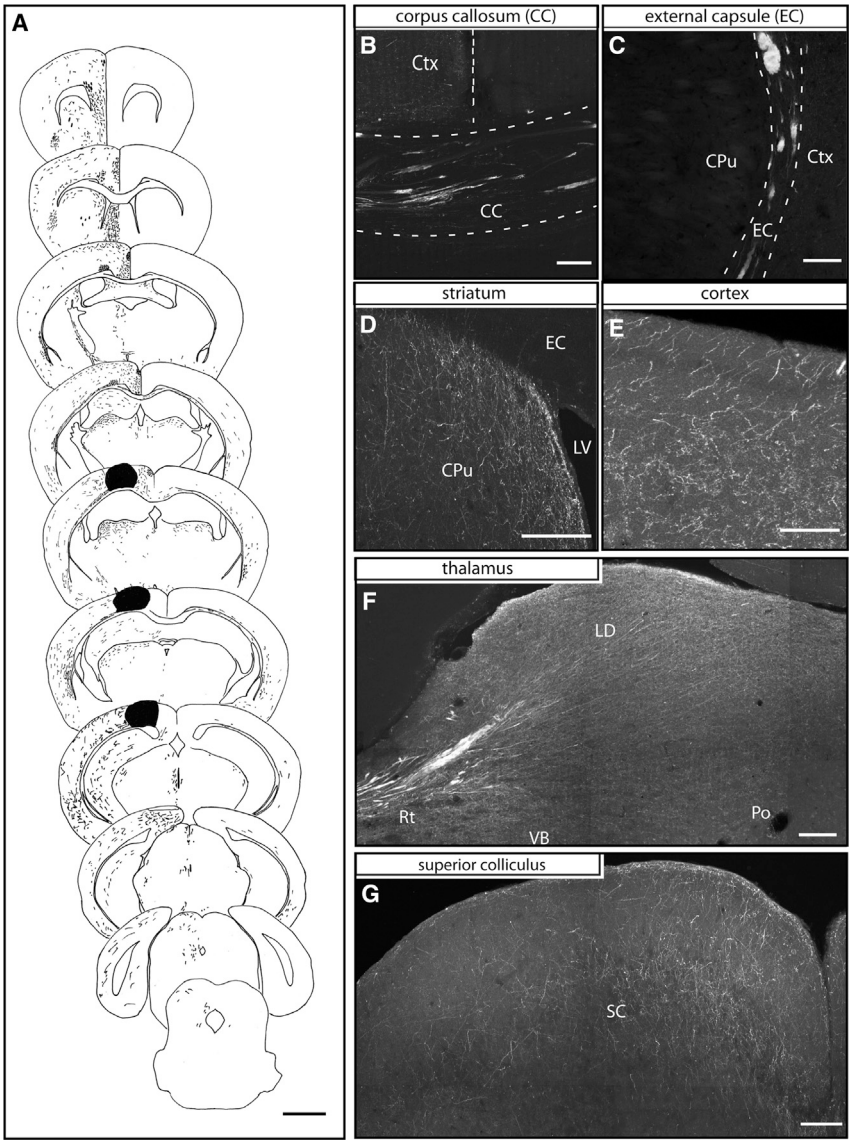


**Figure 2. Human ESC-Derived Cortical Neurons Send Numerous Projections to Specific Cortical Targets following Transplantation into the Adult Murine Visual Cortex**

(A) Camera lucida drawing representing the transplant located into the visual cortex and its projections at 6MPT.

(B–G) GFP$^+$ axonal projections are detected by immunofluorescence in different regions of the mouse brain at 6MPT. Fibers are detected along the corpus callosum (CC) (B) and external capsule (EC) (C). Fibers are also detected in the striatum (CPu) (D), visual cortex (E), thalamus (LD) (F), and superior colliculus (SC) (G).

(F and G) Composite picture views made from the stacked confocal images showing a broad area from thalamus (F) and superior colliculus, midbrain (G). Ctx, cortex; CPu, caudate putamen; LV, lateral ventricle; Rt, reticulate thalamus; LD, laterodorsal thalamic nucleus; VB, ventrobasal complex; Po, posterior thalamic nuclear group.

Scale bars: 2 mm (A), 100 mm (B–G).

axonal outgrowth, with a high number of GFP$^+$ projections located at short- and long-range distances from the graft location, including ipsilateral and contralateral cortical projections (target of layer II-III cortical neurons), and subcortical projections to striatum (target of layer V cortical neurons), thalamus (target of layer VI cortical neurons), and midbrain/hindbrain (target of layer V cortical neurons) (Figure 2).

## Visual Cortical Transplants of Human PSC-Derived Cortical Neurons Display Visual-like Long-Range Axonal Projections in the Adult Brain

Next, we examined in more detail the pattern of projections from the transplants at 6 MPT, especially in terms of areal specificity. We found remarkable areal specificity of the axonal patterns, corresponding to visual and limbic cortex targets, within both cortical and subcortical structures (Figures 3A–3E). In the basal ganglia, transplant-derived projections preferentially targeted the dorsomedial striatum (DM) (a preferential target of visual cortex), rather than the dorsolateral striatum (DL) (preferential target of motor areas) (Figures 2A, 2D, 3A, 3B, and 3F). In the thalamus, transplant-derived axons were detected abundantly within visual/limbic thalamic nuclei (e.g., lateral geniculate nucleus [LG], lateral posterior thalamic nucleus [LP], laterodorsal thalamic nucleus [LD]), while only a minority of fibers were detected in other primary non-visual thalamic nuclei (e.g., ventrobasal complex [VB], posterior thalamic nucleus group [Po], ventrolateral thalamic nucleus [VL], medial geniculate nucleus [MG]) (Figures 2A, 2F, and 3C–3F). Within the midbrain/hindbrain, transplant-derived axonal fibers were detected mostly in the superior colliculus (SC) and periacqueductal gray matter (PAG), which receive mainly inputs from the visual cortex and the limbic cortex, while fewer or no projections were detected in non-visual targets such as the inferior colliculus (IC), pedunculopontine nucleus (PPTg), red nucleus (RedN), and pyramidal tract (Figures 2A, 2G, and 3F). In the contralateral cortex, we also observed projections at the level of the V1/V2 visual cortex and less so at the level of the motor cortex (Figure 2A). A comparison with data from the Allen Mouse Brain Connectivity Atlas following anterograde injection into the V1 visual cortex shows that projections of human transplanted neurons match the normal projections of the visual cortex (Oh et al., 2014).

These data indicate that human PSC-derived cortical neurons transplanted into the lesioned adult visual cortex display a mostly visual-like pattern of axonal projections, which is in line with the patterns observed following neonatal xenotransplantation (Espuny-Camacho et al., 2013) and with what was observed

with transplanted mouse ESC-derived visual-like cortical neurons (Michelsen et al., 2015; Gaspard et al., 2008).

### Long-Range Projections and Transplant Maturation Require a Visual Areal Identity Match

We found that the efficient integration of transplanted mouse ESC-derived cortical neurons or murine embryonic cortical tissue was achieved only if there was a precise match in the areal identity between lesioned and transplanted cells (Gaillard et al., 2007; Michelsen et al., 2015). Therefore, we compared our results obtained with transplants into the visual cortex with the outcome of the transplantations into a non-matching area, the motor cortex at 6 MPT (Figures S3B and S4A). We detected a transplant in 23 of 37 (62%) animals grafted in the motor cortex, including in 82% at 6 MPT, a rate that is slightly higher than that obtained with visual cortex transplantation, while graft volume was not significantly different between visual and motor locations (Figure 4A). However, examination of the pattern of axonal projections revealed that while a similar proportion of transplants projected fibers to the striatum (91% in visual transplants versus 71% in motor-located transplants), fewer motor-located transplants (<50%) sent long-range projections to the thalamic or midbrain/hindbrain levels compared to transplants in the visual cortex (91% in visual transplants versus 47% in motor-located transplants) (Figure 4B). Moreover, quantification of the total number of axonal fibers revealed that motor-located transplants sent far fewer axonal projections to specific subcortical targets, such as LG, LP, LD, SC, and PAG, with the exception of the striatum when compared to visual grafts (Figures 4D and S4B–S4E). It is interesting, however, that the distribution of fibers found in the striatum, thalamus, and midbrain/hindbrain from motor-located transplants also corresponded to a visual areal identity, albeit at a much lower efficiency (Figure 4E).

We then examined in more detail the cellular composition of the transplants in visual versus motor transplants. As expected, both visual and motor-located grafts showed broad expression of the pan-neuronal marker beta 3 class III tubulin (Figures 5A–5F). Notably, the percentage of $Tbr1^+$ or $Foxp2^+$ deep layer cortical neurons was not significantly different between visual versus motor-located grafts (Figure 5G). Alternatively, the expression of mature neuronal and mature glutamatergic markers NeuN and VGlut1 displayed lower levels of expression in motor transplants (Figures 5A–5D). Similarly, Couptf1, an early marker of the occipital cortex (Armentano et al., 2007) that is widely expressed in ESC-derived cortical cells *in vitro* and following their transplantation in the lesioned visual cortex (Espuny-Camacho et al., 2013; Gaspard et al., 2008), also was expressed at lower levels in the motor-located transplants (Figures 5E, 5F, and 5H). Collectively these data indicate that heterotypic transplants in the motor cortex, despite the fact that they contain similar numbers of cortical neurons, fail to re-establish long-range axonal projections and to mature properly at the molecular level.

### Human Transplants in the Visual Cortex Are Synaptically Integrated into the Adult Mouse Brain

To determine whether the transplanted neurons actually integrate at the synapse level, we performed specific marker analyses and patch-clamp recordings. Marker analyses revealed robust expressions of maturation markers for dendrites, axons, and synapses (Figures 6A–6D).

To test functional maturation and synaptic integration, we then performed patch-clamp recordings of transplanted neurons from brain tissue slices prepared from late-stage transplanted animals (8–9 MPT) into the visual cortex. This revealed that the majority of the cells recorded (8 of 13) presented a regular accommodating firing pattern that is characteristic of pyramidal neurons (Figures 6E–6G, S5A, and S5C). Stuttering firing profile, characteristic of some types of cortical interneurons, also was detected in a minority of the cells (3 of 13) (Figure S5B), reflecting that a minority of putative GABAergic cells also was present in the transplants, as shown by Espuny-Camacho et al. (2013. To test whether the grafted human neurons received functional synaptic connections, we measured an electrophysiological correlate of incoming synaptic connectivity. We observed that the human neurons displayed at rest excitatory postsynaptic potentials (EPSPs), present in 3 of 13 cells (Figures 6H and 6I), confirming that the human grafted cells received functional synapses.

Finally, we tested whether the human cells displayed signatures of functional incoming synaptic activity from mouse neuronal networks. We measured their evoked response to a train of extracellular electrical stimuli applied onto mouse host cortical cells located at a distance from the graft. The human neurons (three cells of three tested) showed robust evoked synaptic responses that could be blocked by specific glutamatergic (cyanquixaline [CNQX] and 2-amino-5-phosphonopentanoic acid [AP-V]) and GABAergic (gabazine) receptor antagonists (Figure 6J).

These data indicate that human ESC-derived cortical neurons transplanted into the adult mouse cortex present a mature electrical neuronal profile and are effectively integrated into the glutamatergic and GABAergic adult mouse host circuitry at 8 MPT.

## DISCUSSION

Cell replacement has been proposed and tested as a promising therapeutic avenue for diseases characterized by specific neuronal loss, in particular, Parkinson disease (Aboody et al., 2011; Barker et al., 2015; Tabar and Studer, 2014), but whether this approach could be applied to the loss of a wide diversity of cells in complex structures such as the cerebral cortex is much less clear to date (Goldman, 2016). Here, we differentiated human visual-like cortical projection pyramidal neurons and transplanted them into the lesioned adult murine cortex to test whether these cells could contribute to the reassembly of damaged cortical areas. We found that the human cortical neurons integrated stably into the host-damaged cortex, expressed molecular markers specific for different cortical layer neurons, displayed robust and specific long-range subcortical axonal projections corresponding to the damaged area, and established functional synapses with the host brain.

Efficient brain repair should not only involve axonal outgrowth and the generation of synapses but also, most important, should result in appropriate specificity in connectivity that would resemble closely the damaged circuits that need to be re-established. It is important to note in this context that we report that the pattern of axonal projections from human neurons transplanted into the lesioned visual cortex corresponds to a visual

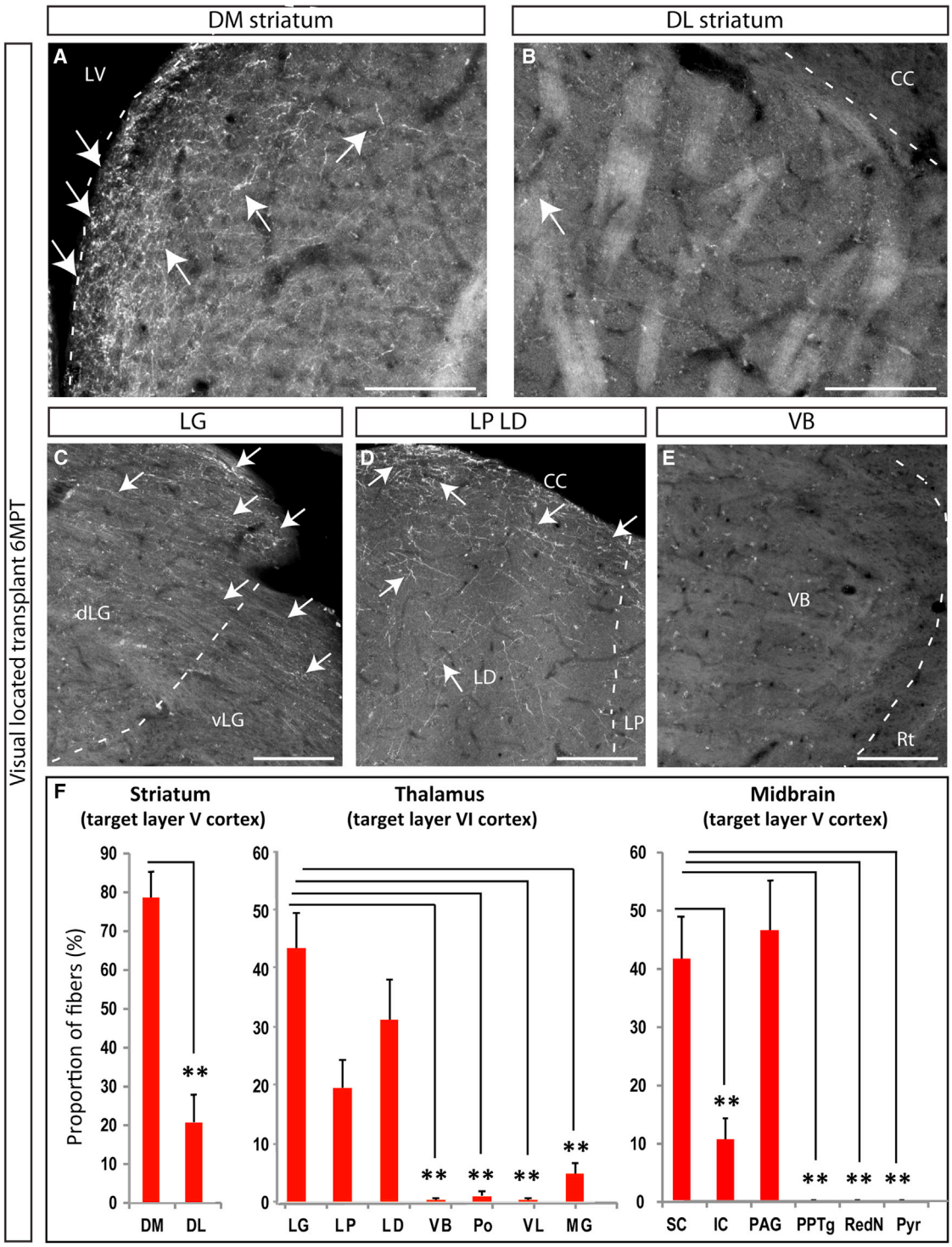


**Figure 3. Human ESC-Derived Cortical Neurons Grafted onto the Visual Cortex Display Specific Visual Cortex-like Projections 6 MPT**

(A and B) Immunofluorescence images showing numerous GFP$^+$ axons in the visual cortical target DM striatum (A) and fewer in the DL striatum (B), which is the target of the motor cortex.

(C–E) GFP$^+$ axons also are detected in the targets of the visual cortex LG (C), LP, and LD (D) (thalamus) and fewer in the somatosensory-motor cortical target VB (thalamus) (E). DM, dorsomedial striatum; DL dorsolateral striatum; LV, lateral ventricle; CC, corpus callosum; dLG, dorsolateral geniculate nucleus; vLG, ventrolateral geniculate nucleus; LD, laterodorsal thalamic nucleus; LP, lateral posterior thalamic nucleus; VB, ventrobasal complex; Rt, reticulate thalamus.

*(legend continued on next page)*

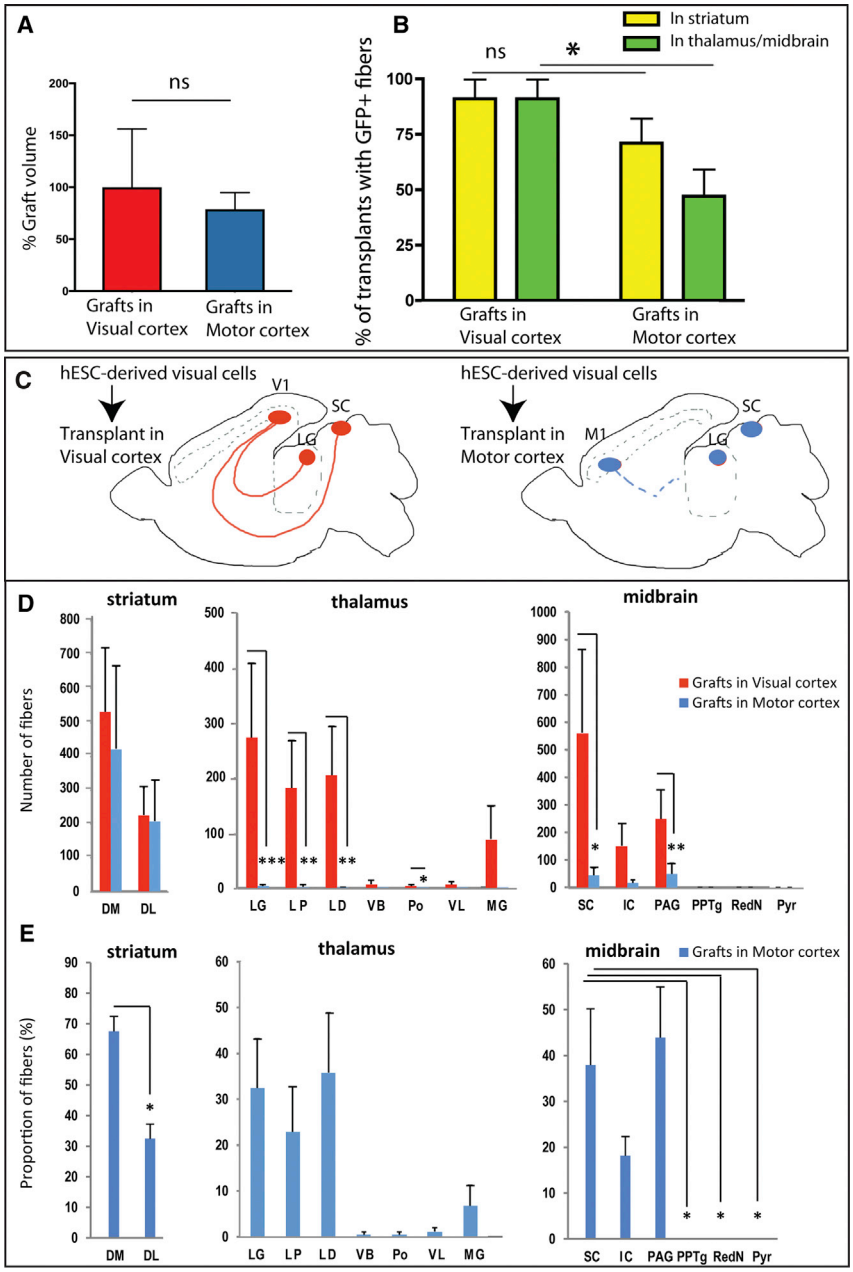


**Figure 4. Successful Graft Integration of hPSC-Derived Neurons into the Lesioned Adult Murine Cortex Requires an Areal Identity Match**

(A) Quantification of the graft volume of human transplants located in the visual cortex or the motor cortex. Data are represented as mean percentages ± SEMs, compared to the value in visual grafts as 100 (n = 8 animals with visual cortex grafts; n = 8 animals with motor cortex grafts). Student's t test; ns = non-significant.

(B) Quantification of the proportion of human transplants presenting GFP$^+$ fibers in striatum (yellow bars) and thalamus and midbrain (green bars) from the total number of grafts located in the visual cortex or in the motor cortex. Data are represented as mean percentages ± SEPs (n = 11 animals with visual cortex grafts and n = 17 animals with motor cortex grafts). Z test; ns = non-significant; *p < 0.05.

(C) Schematic illustration of the pattern of axonal projections obtained following grafting of human visual cells into the adult visual cortex (V1) (left) or the motor cortex (M1) (right).

(D) Quantification of the total number of fibers in the striatum, thalamus, and midbrain/hindbrain of grafts located in the visual cortex or the motor cortex 6 MPT. Data are represented as SEMs (n = 11 animals with visual cortex grafts; n = 17 animals with motor cortex grafts). Mann-Whitney non-parametric test for unpaired data; *p < 0.05; **p < 0.01; ***p < 0.001.

(E) Quantification of the proportion of GFP$^+$ fibers in the striatum, thalamus, and midbrain/hindbrain of grafts located in the motor cortex at 6 MPT. Data are represented as mean percentages ± SEMs (n = 8 animals with motor cortex grafts). Wilcoxon's non-parametric test for paired data; *p < 0.05. DM, dorsomedial striatum; DL, dorsolateral striatum; LG lateral geniculate nucleus; LP, lateral posterior thalamic nucleus; LD, laterodorsal thalamic nucleus; VB, ventrobasal complex; Po, posterior thalamic nuclear group; VL, ventrolateral thalamic nucleus; MG, medial geniculate nuclei of the thalamus; SC, superior colliculus; IC, inferior colliculus; PAG, periaqueductal grey matter; PPTg, pedunculopontine nucleus; RedN, red nucleus; Pyr, pyramidal tract.

cortical identity, thus potentially contributing to the reassembly of damaged visual pathways. These findings are in accordance with what we previously reported with mouse ESC-derived cortical cells transplanted into the lesioned adult visual cortex (Michelsen et al., 2015) and with transplants prepared from mouse embryonic cortex (Gaillard et al., 2007).

These data suggest that the human cortical progenitors and neurons, similar to those in the mouse, acquired a visual cortical identity *in vitro* that was maintained following adult transplantation, thereby allowing area-specific re-establishment of visual axonal pathways.

Moreover, we observed that successful transplantation was obtained only following transplantation in the visual cortex, suggesting that areal identity match may be an important factor for successful cortical transplantation, as previously

(F) Quantification of the proportion of GFP$^+$ fibers detected in the striatum, thalamus, and midbrain/hindbrain of grafts located into the visual cortex at 6 MPT. Data are represented as mean percentages ± SEMs (n = 10 animals). Wilcoxon's non-parametric test for paired data; **p < 0.01. LG, lateral geniculate nucleus; Po, posterior thalamic nuclear group; VL, ventrolateral thalamic nucleus; MG, medial geniculate nuclei of the thalamus; SC, superior colliculus; IC, inferior colliculus; PAG, periaqueductal grey matter; PPtg, pedunculopontine nucleus; RedN, red nucleus; Pyr, pyramidal tract.
Scale bars: 100 μm.

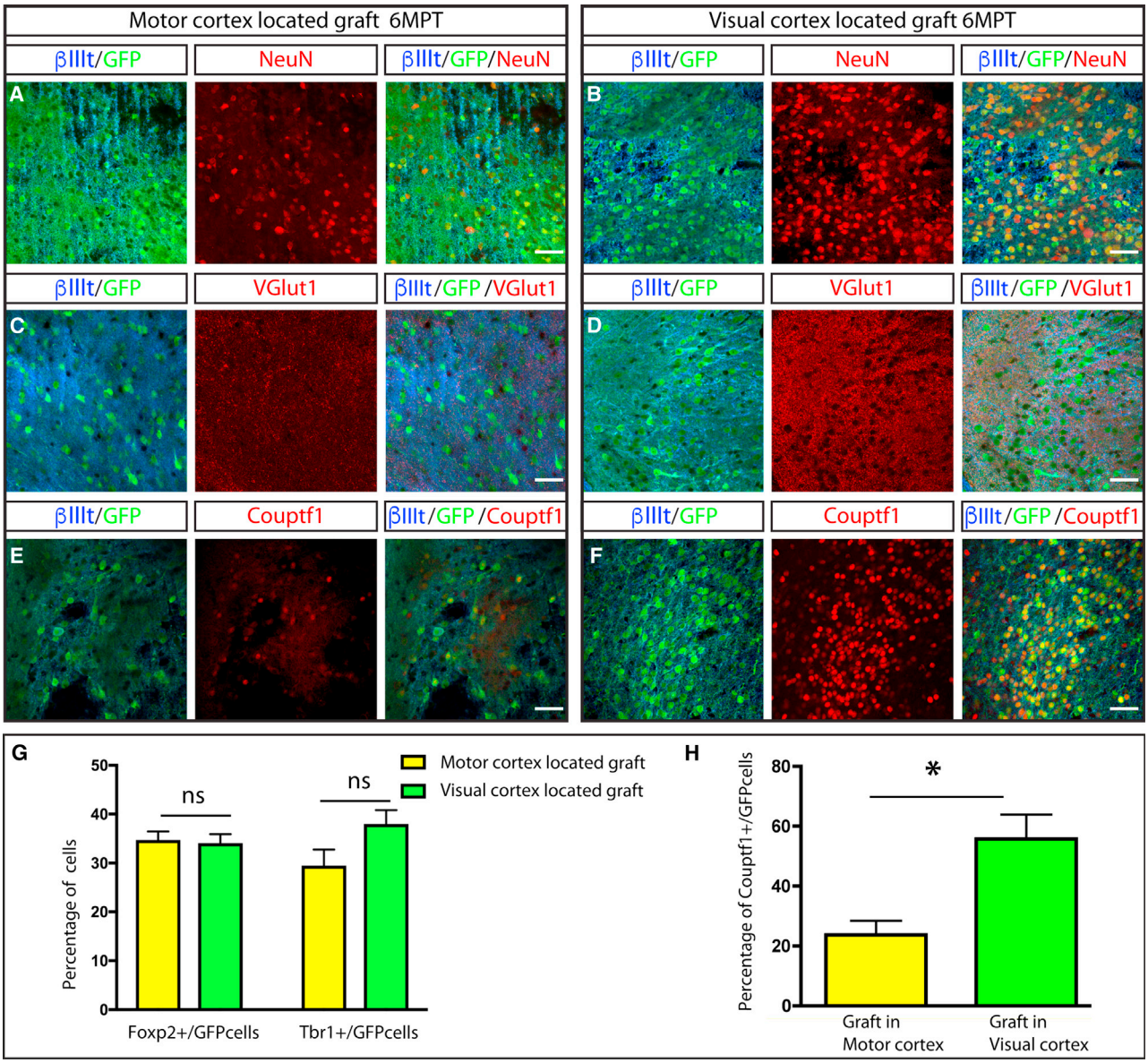


**Figure 5. Visual Cortex Transplants of Human ESC-Derived Neurons Show Mature Neuronal, Glutamatergic, and Visual Cortical Markers at 6 MPT**

(A–F) Immunofluorescence images showing the GFP$^+$ graft (green), beta 3 class III tubulin (blue), and the mature neuronal marker NeuN (red; A and B); the glutamatergic marker VGlut1 (red; C and D); and the visual cortical marker Couptf1 (red; E and F) following transplantation into the motor cortex (A, C, and E) or the visual cortex (B, D, and F) at 6 MPT.

(G) Quantification of the percentage of Tbr1$^+$ and Foxp2$^+$ cells among total GFP$^+$ cells found in grafts located in the motor or the visual cortex. Data are represented as mean percentages ± SEMs (n = 4 animals with visual cortex graft; n = 4 animals with motor cortex graft). Student's t test; ns = non-significant.

(H) Quantification of the percentage of Couptf1$^+$ cells among total GFP$^+$ cells found in grafts located in the motor cortex or the visual cortex. Data are represented as means ± SEMs (n = 3 animals with visual cortex graft; n = 3 animals with motor cortex graft). Student's t test; *p < 0.05.

Scale bars: 50 μm.

observed with transplanted mouse cortical cells (Gaillard et al., 2007; Michelsen et al., 2015). Human ESC-derived neurons were previously transplanted in damaged rodent cortex and displayed evidence of synaptic input from the host brain and improved functional recovery (Tornero et al., 2013, 2017), but they showed little apparent ability to send long-range axonal projections. The latter is reminiscent of our data obtained in the motor cortex transplantation and may be the result of lack of identity match between transplanted cells and the lesioned area.

Conversely, our results contrast with several studies using, for instance, human neural stem cell transplantations that led to

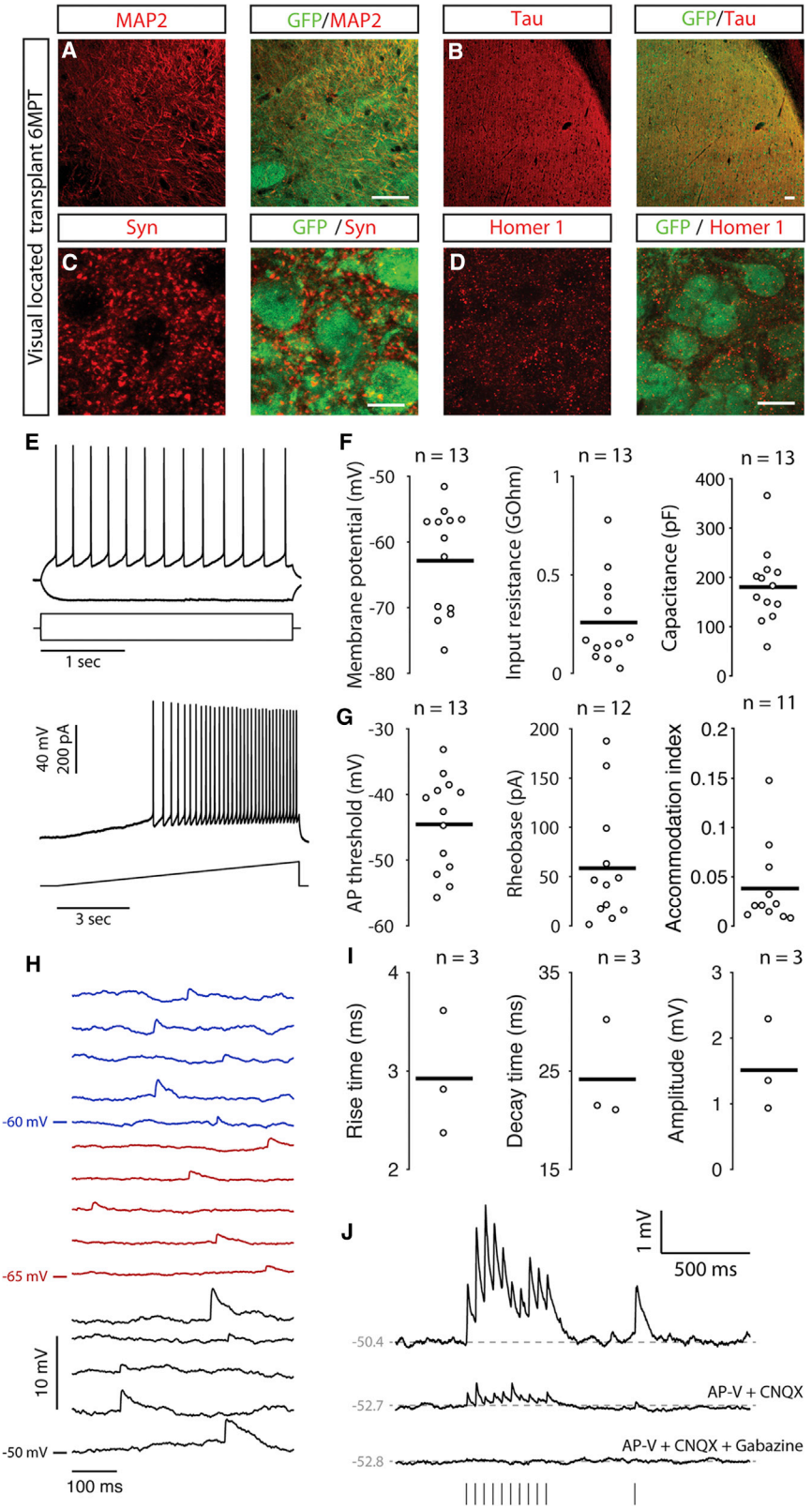


**Figure 6. Functional Maturation of Transplanted Human ESC-Derived Cortical Neurons**

(A–D) Immunofluorescence images showing the GFP$^+$ graft (green) and the dendritic marker MAP2 (red; A); the axonal marker Tau (red; B); the presynaptic marker synaptophysin Syp (red; C), and the postsynaptic marker Homer1 (red; D). Scale bars: 50 μm (A and B) and 10 μm (C and D).

(E) Sample membrane voltage traces of a cell evoked by the intracellular injection of hyperpolarizing and depolarizing current steps (top) and of a 10-s-long ramp current (bottom).

(F and G) Single-cell passive (F) and active (G) membrane properties. Open circles correspond to individual cells, with the bar representing the population mean. Both passive and active properties are in the ranges that are observed typically in cortical pyramidal neurons.

(H) Membrane voltage traces recorded intracellularly from three different cells (blue, red, and black) in current-clamp mode—without injection of any offset current—display EPSPs (n = number of cells for which the specific properties were determined.

(I) Spontaneous EPSPs properties, extracted by fitting each spontaneous event with a double-exponential function. Open circles are averages of all of the events recorded in individual cells (n = 3 cells with significant spontaneous synaptic activity), with the bar representing the population mean.

(J) Sample membrane voltage responses of a neuron (same cell as in H, black traces) evoked by a train of 10 extracellular electrical stimuli repeated at 20 Hz, with a last "recovery" pulse at 500 ms delivered after the last pulse in the train. All of the traces represent the average responses for 20–30 repetitions. The top trace shows the evoked response during perfusion with standard aCSF. The application of selective competitive antagonists of α-amino-3-hydroxyl-5-methyl-4-isoxazole-propionate (AMPA) and *N*-methyl-D-aspartate (NMDA) receptors (CNQX and AP-V, respectively) blocks the glutamatergic responses, significantly suppressing the evoked PSPs (central trace). The residual response was $GABA_A$ receptor mediated, as demonstrated by its abolishment following application of the $GABA_A$ receptor antagonist gabazine (bottom trace).

successful patterns of connectivity with the same cells independent of the sites of transplantation (Doerr et al., 2017; Steinbeck et al., 2012; Wernig et al., 2004). The differences could be caused by distinct degrees of fate specification before transplantation. Completely fated cortical cells, such as the ones used in this study, do not display much capacity to be influenced by or adapt to the host adult brain, while other "earlier" types of neural stem cells that are less committed may be more capable of doing so, as shown with mouse embryonic cortex (Gaillard et al., 2003). These and our current data emphasize the importance of determining the underlying mechanisms regulating fate acquisition, maintenance, and plasticity following transplantation because these could have key implications for successful transplantation in clinical settings. In addition, it will be important to test further the relevance and importance of areal identity match by testing the efficiency of human motor cortex-fated cells transplanted in motor versus non-motor cortex locations, as was done with mouse embryonic cortical cells (Gaillard et al., 2007).

Conversely, it will be interesting to determine whether and how molecular cues could be involved in the apparent area specificity observed following adult transplantation. While it seems unlikely that the re-establishment of damaged axonal pathways strictly recapitulates developmental events, it is tempting to speculate that specific guidance cues normally acting during embryogenesis (Vanderhaeghen and Polleux, 2004) may be residually expressed or re-expressed following lesions (e.g., on remaining axons), thereby allowing the reassembly of lost neural circuits with the observed specificity. In addition, it will be interesting to test whether specific patterns of neural activity could contribute to the area-specific re-establishment of damaged pathways, as they do in normal development (Sur and Rubenstein, 2005).

In addition to long-range projections, the transplanted human cortical neurons displayed electrophysiological properties that indicate their functional maturation and integration with the host brain. However, much work remains to be done to determine whether these neurons can function in a physiologically relevant way, in this case to subserve visual function, as recently shown for mouse embryonic cortex-derived transplanted neurons (Falkner et al., 2016).

Moreover, while the use of visual neurons appears to be a fruitful model to study function in an experimental setting, from a therapeutic point of view, it will be important to be able to generate human cortical neurons of other areal identities, such as motor and somatosensory, and test their relevance for the restoration of motor function (e.g., as would be mostly required following stroke or brain trauma). The ability to obtain motor cortex-fated cells is still missing in the field and will require a thorough exploration of the spatial patterning cues that control cortical neuronal fate *in vivo* and *in vitro* (Sur and Rubenstein, 2005). Another exciting approach would be to try to combine the transplantation of cortical pyramidal neurons with cortical interneurons, because the latter also have been shown to be able to integrate following transplantation (Anderson and Vanderhaeghen, 2014; Cunningham et al., 2014; Maroof et al., 2013; Nicholas et al., 2013). Finally, it will be interesting to study the temporal aspect of human corticogenesis following transplantation in the adult brain. Indeed, as observed for neonatal transplantation (Qi et al., 2017; Espuny-Camacho et al., 2013, 2017), human neurons mature and integrate into adult neural circuits only following MPT. Human neurons transplanted in the neonatal or adult brain appear to mature functionally following their own time-specific pace, reminiscent of the neoteny that characterizes human cortical synaptogenesis (Defelipe, 2011; Suzuki and Vanderhaeghen, 2015). Such a slow speed may constitute a hurdle for an efficient use in clinical settings, although it may be necessary to achieve the reassembly of neural circuits in a physiologically relevant way.

In conclusion, we show here that human cortical projection neurons can be efficiently transplanted into the lesioned rodent cortex, with a specificity that may be highly relevant for the repair of defined lesions of cortical areas. These data constitute an important proof of principle to explore the possibilities and mechanisms underlying the reconstruction of lost neuronal circuits in the adult mammalian brain.

## EXPERIMENTAL PROCEDURES

### Human ESC Differentiation into Cortical Cells

For the differentiation of human ESCs toward cortical progenitors and neurons (Espuny-Camacho et al., 2013), cells were dissociated using StemPro Accutase on day 2 (Invitrogen, catalog no. A11105) and plated on Matrigel (BD, human ESC-qualified Matrigel)-coated coverslips/dishes at low confluency (5,000–10,000 cells/cm$^2$) in MEF-conditioned human ESC/human iPSC medium supplemented with rho-associated protein kinase (ROCK) inhibitor (Y-27632; 10 μM Calbiochem, Sigma-Aldrich, catalog no. 688000). On day 0 of the differentiation, the medium was changed to default differentiation medium (DDM) (Gaspard et al., 2008) supplemented with B27 (10 mL B27 per 500 mL DDM, GIBCO) and Noggin (100 ng/mL, R&D Systems) (Espuny-Camacho et al., 2013). At 16 days *in vitro* (DIV), Noggin was withdrawn and the medium was changed to DDM and supplemented with B27 (GIBCO). At 24 DIV the human cortical progenitors were manually dissociated and a dilution of 100,000 cells/μL was prepared for transplantation experiments, as described by Espuny-Camacho et al. (2013).

### Mice Lesioning and Grafting

All of the animal experiments were carried out in full compliance with the Université Libre de Bruxelles Committee for animal welfare and Belgian and European regulations. Data for this study are derived from a total of 58 adult mice of both sexes (n = 37 for motor-located transplants and n = 21 for visual-located transplants). Lesioning and grafting experiments were performed in 6- to 8-week old adult NOD/SCID mice, as described by Michelsen et al. (2015). Lesioning was performed under anesthesia by focal stereotactic injections of ibotenic acid either in the visual or motor cortex (20 mg of ibotenic acid in 1 μL distilled water; see Supplemental Experimental Procedures for coordinates). Three days after lesioning, approximately 100,000 human ESC-derived cortical progenitors (in 0.5–1 μL) were injected in the visual or the motor cortex.

### Quantification of Axonal Projections

GFP$^+$ fibers were quantified using a Zeiss Axioplan upright fluorescence microscope equipped with 20x and 40x dry objectives. The GFP was enhanced by immunofluorescence staining against GFP. For the striatum, the total number of fibers was counted in one-sixth of the coronal sections collected for each individual brain. For the thalamus and midbrain, fibers were counted in half of the coronal sections collected for each individual brain. Data are represented as means ± SEMs. For the percentage of fibers, 10 and 8 animals were used for quantification following transplantation into the visual and motor cortex, respectively. For the total number of fibers in visual and motor transplants, 11 and 17 animals were used for quantification following transplantation into the visual cortex and the motor cortex, respectively.

### Quantification of the Tbr1, Foxp2, and Couptf1 Cells in Transplants

The percentage of Tbr1$^+$, Foxp2$^+$, and Couptf1$^+$ cells detected among the total number of GFP$^+$ cells (human grafted cells) was counted on confocal acquired images from immunofluorescence stained brain sections. Data are represented as mean percentages ± SEMs (n = 4−3 animals grafted into the visual cortex; n = 4−3 animals grafted into the motor cortex).

### Quantification of Graft Volume

The graft volume was measured from confocal images from the graft in serial coronal sections corresponding to one-sixth of the mouse brain. Mouse brain sections were immunostained with GFP antibody and z stacks of 10 μm were acquired for a total of 6 steps (60 μm thickness). The volume of the graft was calculated using Fiji software. Data are represented as mean percentages ± SEMs (n = 8 animals grafted into the visual cortex; n = 8 animals grafted into the motor cortex).

### Quantification of the Proportion of Transplants with Subcortical Projections

The proportion of visual and motor-located transplants projecting GFP$^+$ fibers into the striatum, thalamus, or midbrain/hindbrain was quantified by manual counting from immunofluorescence stained brain sections using the GFP antibody. Data are represented as mean percentages ± SE of the proportions (SEPs) (visual grafts: n = 11 animals; motor grafts: n = 17 animals).

### Brain Tissue Slice Electrophysiology

Electrophysiological recordings were performed intracellularly on grafted neurons in acute brain slices from mice at 8 and 9 MPT as previously described (Espuny-Camacho et al., 2013). Briefly, 300-μm thick coronal slices were cut in a sucrose-based solution and subsequently stored in artificial cerebrospinal fluid (aCSF) before recording. Transplanted cells were identified by their EGFP fluorescence and visualized using an upright microscope equipped with infrared differential interference contrast (DM LFS, Leica Microsystems). Whole-cell patch-clamp recordings and bipolar extracellular stimulation were performed and analyzed as described in more detail in the Supplemental Experimental Procedures.

#### *Statistics*

Statistical analyses were performed using PRISM (GraphPad). Appropriate statistical tests were chosen in each case depending on sample size, data distribution, and number of comparisons. The percentage of axonal projections in different subcortical targets for visual or motor transplants was analyzed using the non-parametric Wilcoxon signed-rank test for paired data, with *$p < 0.05 <$ and **$p < 0.01$. The total number of fibers in visual and motor transplants was analyzed using the non-parametric Mann-Whitney test for unpaired data, with *$p < 0.05 <$, **$p < 0.01$, and ***$p < 0.001$. The proportion of Tbr1$^+$, Foxp2$^+$, and Couptf1$^+$ cells was analyzed by Student's t test; n.s. = non-significant; *$p < 0.05$. The proportion of graft volume in motor and visual transplants was analyzed by Student's t test; n.s. = non-significant. The proportion of transplants with subcortical projections was performed following the Z test for proportions; ns = non-significant; *$p < 0.05$.

### Additional Methods

An extended version of the experimental procedures is described in the Supplemental Experimental Procedures.

## SUPPLEMENTAL INFORMATION

Supplemental Information includes Supplemental Experimental Procedures and five figures and can be found with this article online at https://doi.org/10.1016/j.celrep.2018.04.094.

## ACKNOWLEDGMENTS

We thank members of the laboratory and IRIBHM for helpful feedback and support and Jean-Marie Vanderwinden of the Light Microscopy Facility (LiMiF) for support with imaging. We also thank Chiara Cordiglieri from INGM Imaging for support with 3D image analysis. This work was funded by grants from the Belgian Fund for Scientific Research (FNRS), the Belgian Queen Elizabeth Medical Foundation, the Interuniversity Attraction Poles Program (IUAP), the WELBIO Program of the Walloon Region, the European Research Council (ERC-2013-AG-340020), the AXA Research Fund, the Fondation ULB, the VIB, and KULeuven (to P.V.) and the Flanders Research Foundation (FWO) (grant no. G0F1517N to M.G.). I.E.-C. was a post-doctoral fellow of the FNRS.

## AUTHOR CONTRIBUTIONS

I.E.-C. performed all of the differentiation and transplantation experiments with the help of A.G., K.A.M., A.B., S.A.-V., and A.H. K.A.M. performed the axon fiber quantifications. D.L. performed the electrophysiological recordings. I.E.-C. and P.V. wrote the manuscript. P.V., A.G., M.G., and I.E.-C. designed and analyzed all of the experiments.

## DECLARATION OF INTERESTS

The authors declare no competing interests.

Received: August 4, 2017
Revised: March 9, 2018
Accepted: April 23, 2018
Published: May 29, 2018

## REFERENCES

Aboody, K., Capela, A., Niazi, N., Stern, J.H., and Temple, S. (2011). Translating stem cell studies to the clinic for CNS repair: current state of the art and the need for a Rosetta stone. Neuron *70*, 597–613.

Anderson, S., and Vanderhaeghen, P. (2014). Cortical neurogenesis from pluripotent stem cells: complexity emerging from simplicity. Curr. Opin. Neurobiol. *27*, 151–157.

Arlotta, P., and Berninger, B. (2014). Brains in metamorphosis: reprogramming cell identity within the central nervous system. Curr. Opin. Neurobiol. *27*, 208–214.

Armentano, M., Chou, S.-J., Tomassy, G.S., Leingärtner, A., O'Leary, D.D.M., and Studer, M. (2007). COUP-TFI regulates the balance of cortical patterning between frontal/motor and sensory areas. Nat. Neurosci. *10*, 1277–1286.

Barker, R.A., Drouin-Ouellet, J., and Parmar, M. (2015). Cell-based therapies for Parkinson disease—past insights and future potential. Nat. Rev. Neurol. *11*, 492–503.

Cunningham, M., Cho, J.H., Leung, A., Savvidis, G., Ahn, S., Moon, M., Lee, P.K.J., Han, J.J., Azimi, N., Kim, K.S., et al. (2014). hPSC-derived maturing GABAergic interneurons ameliorate seizures and abnormal behavior in epileptic mice. Cell Stem Cell *15*, 559–573.

Defelipe, J. (2011). The evolution of the brain, the human nature of cortical circuits, and intellectual creativity. Front. Neuroanat. *5*, 29.

Doerr, J., Schwarz, M.K., Wiedermann, D., Leinhaas, A., Jakobs, A., Schloen, F., Schwarz, I., Diedenhofen, M., Braun, N.C., Koch, P., et al. (2017). Whole-brain 3D mapping of human neural transplant innervation. Nat. Commun. *8*, 14162.

Eiraku, M., Watanabe, K., Matsuo-Takasaki, M., Kawada, M., Yonemura, S., Matsumura, M., Wataya, T., Nishiyama, A., Muguruma, K., and Sasai, Y. (2008). Self-organized formation of polarized cortical tissues from ESCs and its active manipulation by extrinsic signals. Cell Stem Cell *3*, 519–532.

Espuny-Camacho, I., Michelsen, K.A., Gall, D., Linaro, D., Hasche, A., Bonnefont, J., Bali, C., Orduz, D., Bilheu, A., Herpoel, A., et al. (2013). Pyramidal neurons derived from human pluripotent stem cells integrate efficiently into mouse brain circuits in vivo. Neuron *77*, 440–456.

Espuny-Camacho, I., Arranz, A.M., Fiers, M., Snellinx, A., Ando, K., Munck, S., Bonnefont, J., Lambot, L., Corthout, N., Omodho, L., et al. (2017). Hallmarks of Alzheimer's disease in stem-cell-derived human neurons transplanted into mouse brain. Neuron *93*, 1066–1081.e8.

Falkner, S., Grade, S., Dimou, L., Conzelmann, K.-K., Bonhoeffer, T., Götz, M., and Hübener, M. (2016). Transplanted embryonic neurons integrate into adult neocortical circuits. Nature *539*, 248–253.

Gage, F.H., and Temple, S. (2013). Neural stem cells: generating and regenerating the brain. Neuron *80*, 588–601.

Gaillard, A., Nasarre, C., and Roger, M. (2003). Early (E12) cortical progenitors can change their fate upon heterotopic transplantation. Eur. J. Neurosci. *17*, 1375–1383.

Gaillard, A., Prestoz, L., Dumartin, B., Cantereau, A., Morel, F., Roger, M., and Jaber, M. (2007). Reestablishment of damaged adult motor pathways by grafted embryonic cortical neurons. Nat. Neurosci. *10*, 1294–1299.

Gascón, S., Masserdotti, G., Russo, G.L., and Götz, M. (2017). Direct neuronal reprogramming: Achievements, hurdles and new roads to success. Cell Stem Cell *21*, 18–34.

Gaspard, N., Bouschet, T., Hourez, R., Dimidschstein, J., Naeije, G., van den Ameele, J., Espuny-Camacho, I., Herpoel, A., Passante, L., Schiffmann, S.N., et al. (2008). An intrinsic mechanism of corticogenesis from embryonic stem cells. Nature *455*, 351–357.

Goldman, S.A. (2016). Stem and progenitor cell-based therapy of the central nervous system: hopes, hype, and wishful thinking. Cell Stem Cell *18*, 174–188.

Maroof, A.M., Keros, S., Tyson, J.A., Ying, S.-W., Ganat, Y.M., Merkle, F.T., Liu, B., Goulburn, A., Stanley, E.G., Elefanty, A.G., et al. (2013). Directed differentiation and functional maturation of cortical interneurons from human embryonic stem cells. Cell Stem Cell *12*, 559–572.

Michelsen, K.A., Acosta-Verdugo, S., Benoit-Marand, M., Espuny-Camacho, I., Gaspard, N., Saha, B., Gaillard, A., and Vanderhaeghen, P. (2015). Area-specific reestablishment of damaged circuits in the adult cerebral cortex by cortical neurons derived from mouse embryonic stem cells. Neuron *85*, 982–997.

Nicholas, C.R., Chen, J., Tang, Y., Southwell, D.G., Chalmers, N., Vogt, D., Arnold, C.M., Chen, Y.J.J., Stanley, E.G., Elefanty, A.G., et al. (2013). Functional maturation of hPSC-derived forebrain interneurons requires an extended timeline and mimics human neural development. Cell Stem Cell *12*, 573–586.

Oh, S.W., Harris, J.A., Ng, L., Winslow, B., Cain, N., Mihalas, S., Wang, Q., Lau, C., Kuan, L., Henry, A.M., et al. (2014). A mesoscale connectome of the mouse brain. Nature *508*, 207–214.

Péron, S., Droguerre, M., Debarbieux, F., Ballout, N., Benoit-Marand, M., Francheteau, M., Brot, S., Rougon, G., Jaber, M., and Gaillard, A. (2017). A delay between motor cortex lesions and neuronal transplantation enhances graft integration and improves repair and recovery. J. Neurosci. *37*, 1820–1834.

Qi, Y., Zhang, X.J., Renier, N., Wu, Z., Atkin, T., Sun, Z., Ozair, M.Z., Tchieu, J., Zimmer, B., Fattahi, F., et al. (2017). Combined small-molecule inhibition accelerates the derivation of functional cortical neurons from human pluripotent stem cells. Nat. Biotechnol. *35*, 154–163.

Shi, Y., Kirwan, P., Smith, J., Robinson, H.P.C., and Livesey, F.J. (2012). Human cerebral cortex development from pluripotent stem cells to functional excitatory synapses. Nat. Neurosci. *15*, 477–486.

Steinbeck, J.A., Koch, P., Derouiche, A., and Brüstle, O. (2012). Human embryonic stem cell-derived neurons establish region-specific, long-range projections in the adult brain. Cell. Mol. Life Sci. *69*, 461–470.

Sur, M., and Rubenstein, J.L.R. (2005). Patterning and plasticity of the cerebral cortex. Science *310*, 805–810.

Suzuki, I.K., and Vanderhaeghen, P. (2015). Is this a brain which I see before me? Modeling human neural development with pluripotent stem cells. Development *142*, 3138–3150.

Tabar, V., and Studer, L. (2014). Pluripotent stem cells in regenerative medicine: challenges and recent progress. Nat. Rev. Genet. *15*, 82–92.

Tornero, D., Wattananit, S., Grønning Madsen, M., Koch, P., Wood, J., Tatarishvili, J., Mine, Y., Ge, R., Monni, E., Devaraju, K., et al. (2013). Human induced pluripotent stem cell-derived cortical neurons integrate in stroke-injured cortex and improve functional recovery. Brain *136*, 3561–3577.

Tornero, D., Tsupykov, O., Granmo, M., Rodriguez, C., Grønning-Hansen, M., Thelin, J., Smozhanik, E., Laterza, C., Wattananit, S., Ge, R., et al. (2017). Synaptic inputs from stroke-injured brain to grafted human stem cell-derived neurons activated by sensory stimuli. Brain *140*, 692–706.

van den Ameele, J., Tiberi, L., Vanderhaeghen, P., and Espuny-Camacho, I. (2014). Thinking out of the dish: what to learn about cortical development using pluripotent stem cells. Trends Neurosci. *37*, 334–342.

Vanderhaeghen, P., and Polleux, F. (2004). Developmental mechanisms patterning thalamocortical projections: intrinsic, extrinsic and in between. Trends Neurosci. *27*, 384–391.

Wernig, M., Benninger, F., Schmandt, T., Rade, M., Tucker, K.L., Büssow, H., Beck, H., and Brüstle, O. (2004). Functional integration of embryonic stem cell-derived neurons in vivo. J. Neurosci. *24*, 5258–5268.

**Cell Reports, Volume *23***

## Supplemental Information

# Human Pluripotent Stem-Cell-Derived Cortical Neurons Integrate Functionally into the Lesioned Adult Murine Visual Cortex in an Area-Specific Way

**Ira Espuny-Camacho, Kimmo A. Michelsen, Daniele Linaro, Angéline Bilheu, Sandra Acosta-Verdugo, Adèle Herpoel, Michele Giugliano, Afsaneh Gaillard, and Pierre Vanderhaeghen**

# Supplemental Materials

## Supplemental Figures

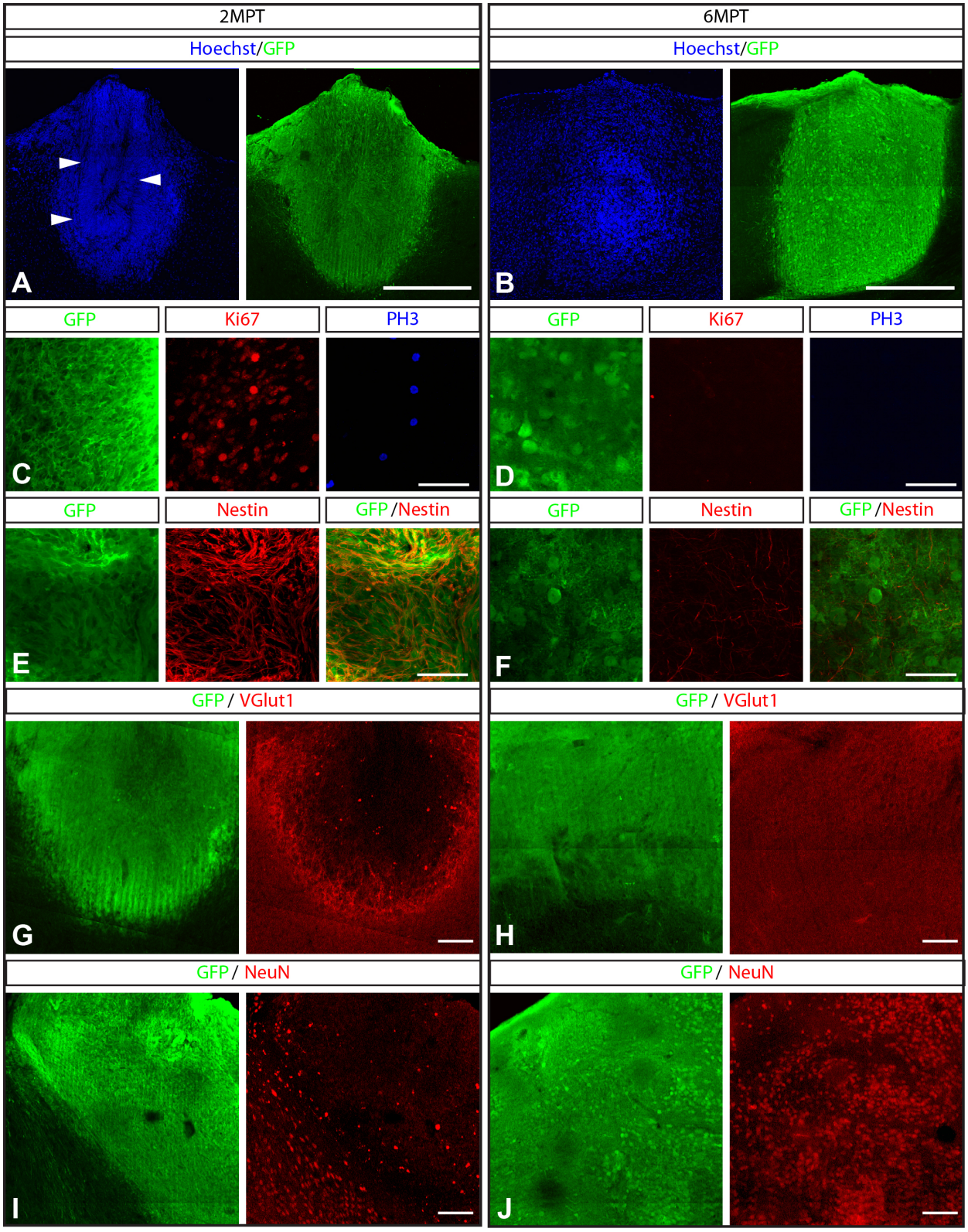


**Figure S1. Gradual maturation of human transplants between 2MPT and 6MPT. Related to Figure 1 and Figure 2**

(A-B) Representative immunofluorescence images of grafts at 2MPT (A) and 6MPT (B) showing the nuclear staining Hoechst (in blue) and the GFP+ graft (in green). Arrowheads show the presence of rosette-like structures at 2MPT. (C-F) Immunofluorescence images showing the GFP+ graft (in green) and the proliferative/progenitor markers Ki67 (in red; C-D), PH3 (in blue; C-D), and Nestin (in red; E-F) at 2MPT (C,E) and 6MPT (E,F). (G-J) Immunofluorescence images showing the GFP+ graft (in green) and the mature neuronal markers VGlut1 (in red; G-H), and NeuN (in red; I-J) at 2MPT (G,I) and 6MPT (H,J). (A-B) Composite picture views made from the stacked confocal images showing the whole transplant after 2MPT (A) and 6MPT (B). Scale bars 500 µm (A-B); 50 µm (C-F); 100 µm (G-J).

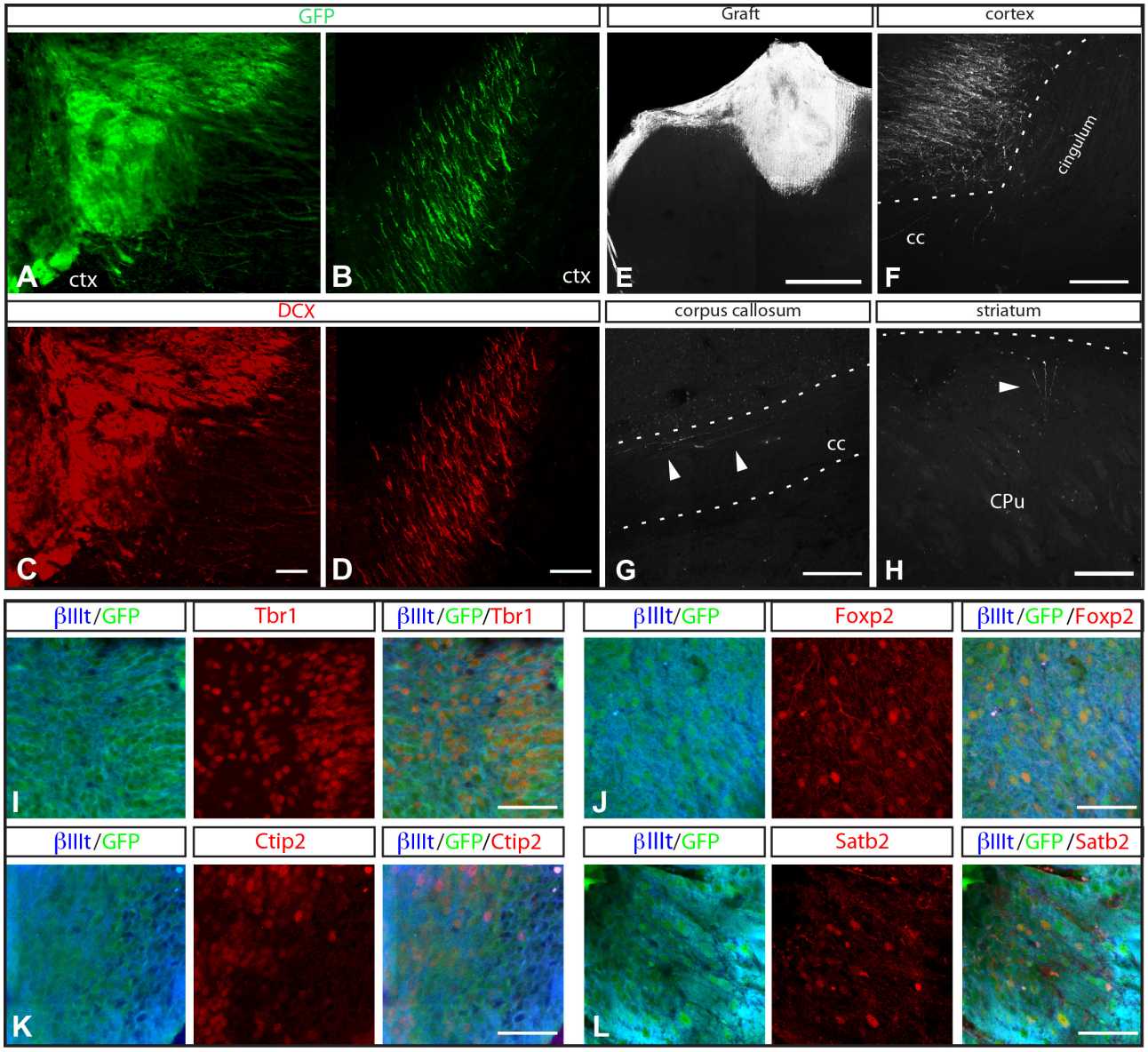


**Figure S2. Transplanted human ESC-derived neurons display short-range axonal projections and immature growth cones at 2MPT. Related to Figure 1 and Figure 2**

(A-D) Immunofluorescence images showing GFP+ somas and GFP+ neural processes (in green; A-B), and the immature neuronal growth cone marker DCX (in red; C-D) in grafted hESC-derived neurons in the cortex 2MPT. (E-H) Immunofluorescence images showing the location of the GFP+ graft (E), neighbouring GFP+ ipsilateral cortical projections (F), and a few fibers along the corpus callosum (G) and in the striatum (H). Arrowheads show the few fibers detected. Ctx, cortex; cc, corpus callosum; CPu, caudate putamen. (I-L) Immunofluorescence images showing the GFP+ graft (in green), beta III tubulin (in blue) and the deep layer cortical neuronal markers Tbr1 (in red; I); Foxp2 (in red; J); Ctip2 (in red; K) and the upper layer cortical neuronal marker Satb2 (in red; L) 2 MPT. (E) Composite picture view made from the stacked confocal images showing the transplant and few fibers 2MPT. cc, corpus callosum; CPu, caudate putamen (striatum). Scale bars 50 μm (A-D; I-L); 500 μm (E); 100 μm (F-H).

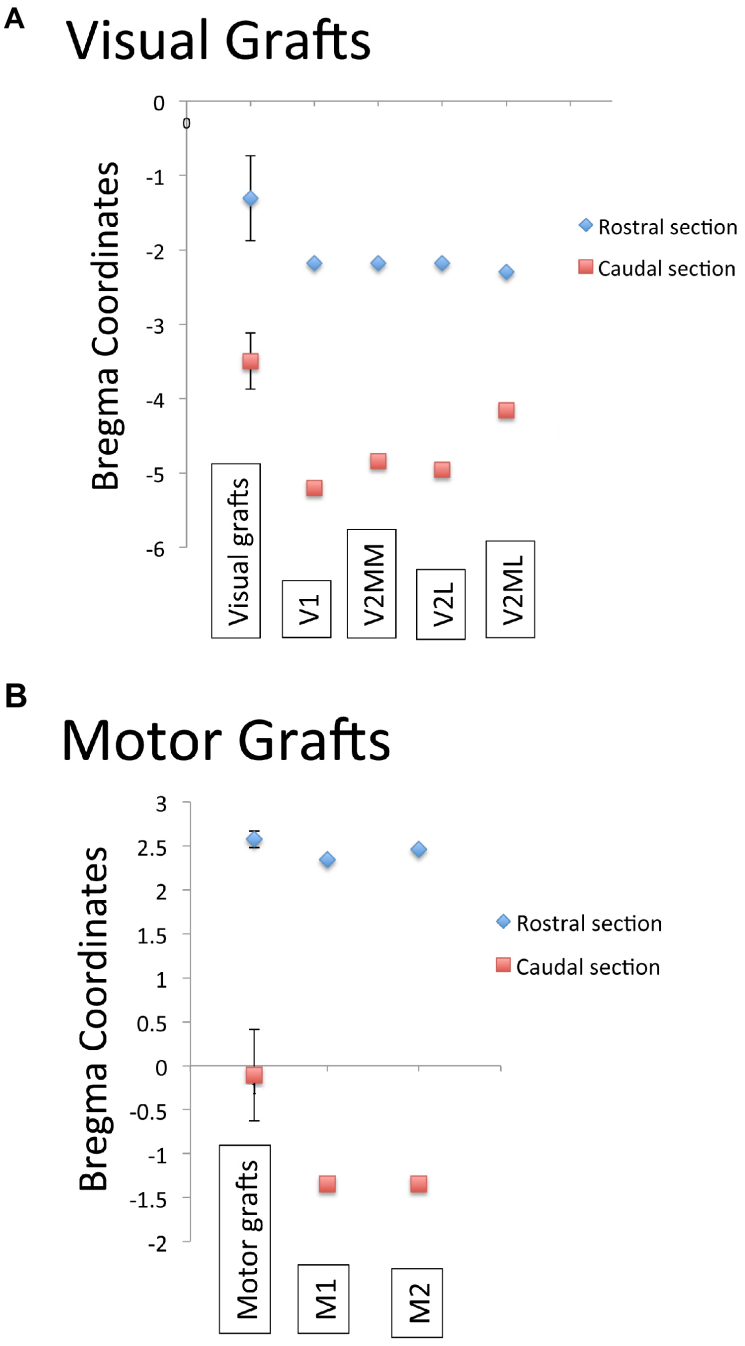


**Figure S3. Transplants into Motor and Visual cortex localize within motor and visual cortical areas, respectively. Related to Figure 4 and Figure 5.**

(A,B) Quantification of the graft bregma coordinates following transplantation into the visual (A) or motor cortex (B) in comparison with the location of visual and motor host cortical areas. Data are presented as mean bregma coordinates ± s.e.m., (n=7 visual grafts; n=4 motor grafts) of the most rostral section (blue diamond symbol) and the most caudal section (red square symbol) of the grafts. The most rostral and the most caudal bregma coordinates of host visual and motor cortical areas are also represented (A-B). V1, primary visual cortex; V2MM, secondary visual cortex, mediomedial area; V2L, secondary visual cortex, lateral area; V2ML, secondary visual cortex, mediolateral area; M1, primary motor cortex; M2, secondary motor cortex.

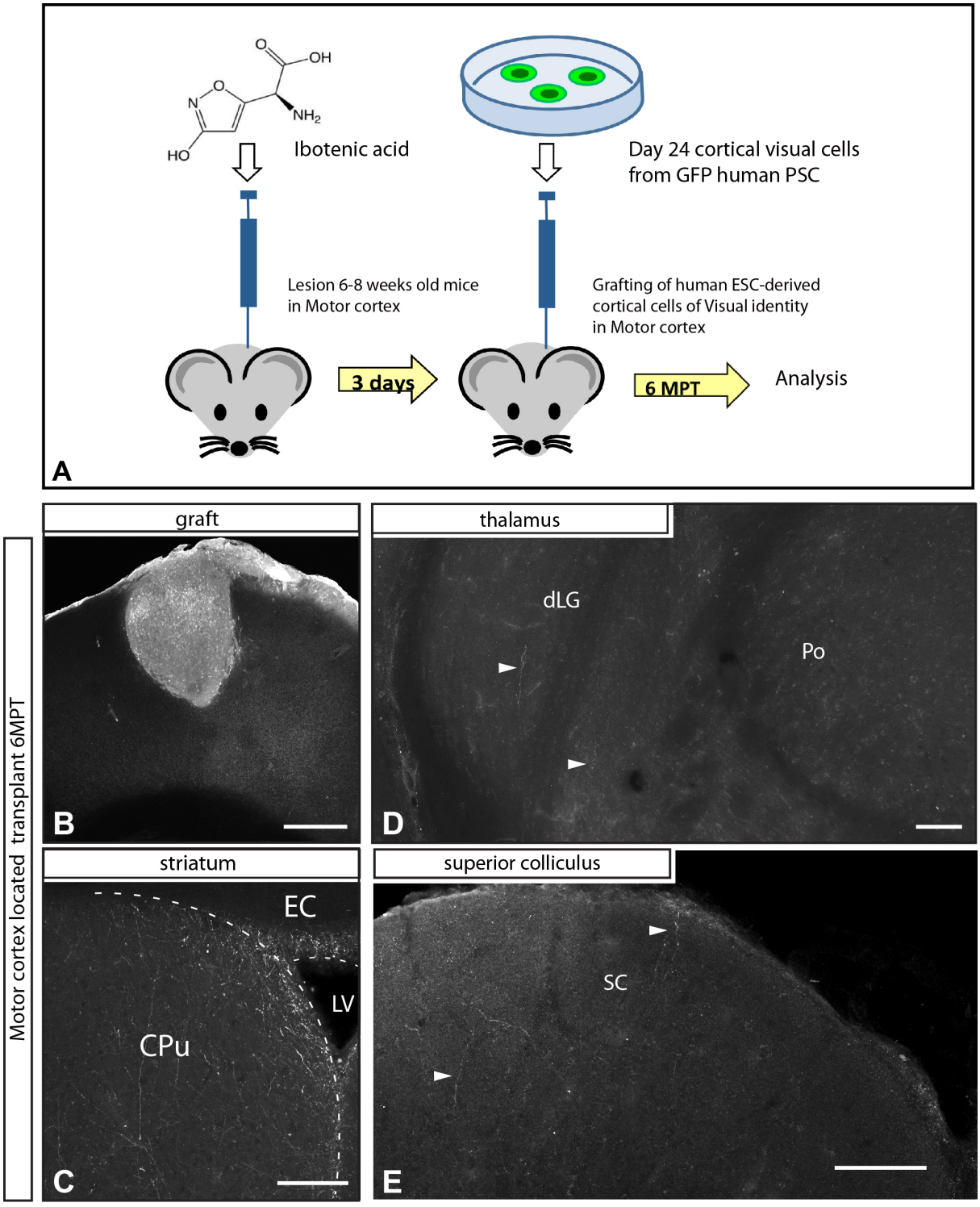


**Figure S4. Transplants into the Motor cortex of human ESC-derived cortical neurons show few long-range projections at 6MPT. Related to Figure 4 and Figure 5.**

(A) Experimental scheme of the lesioning/transplantation experiments in motor cortex. (B) GFP+ graft location is detected by immunofluorescence in the motor cortex at 6MPT. (C-E) Following motor cortex transplantation GFP+ axonal projections are detected by immunofluorescence in different regions of the mouse brain 6MPT. Fibers are detected in the striatum (CPu) (C), however, almost no fibers are detected in thalamic (dLG) (D), or midbrain structures (SC) (E). dLG, dorsal lateral geniculate; Po, posterior nucleus; EC, external capsule; LV, lateral ventricule; CPu, caudate putamen; SC, superior colliculus. (B,D-E) Composite picture views made from the stacked confocal images showing the whole transplant located into the motor cortex (B), dLG and Po, thalamus (D), and the superior colliculus, midbrain (E) at 6MPT. dLG, dorsolateral geniculate nucleus; Po, posterior thalamic nuclear group; CPu, caudate putamen; ec, external capsule; LV, lateral ventricle; SC, superior colliculus. Scale bars 500 µm (B), 100 µm (B-D).

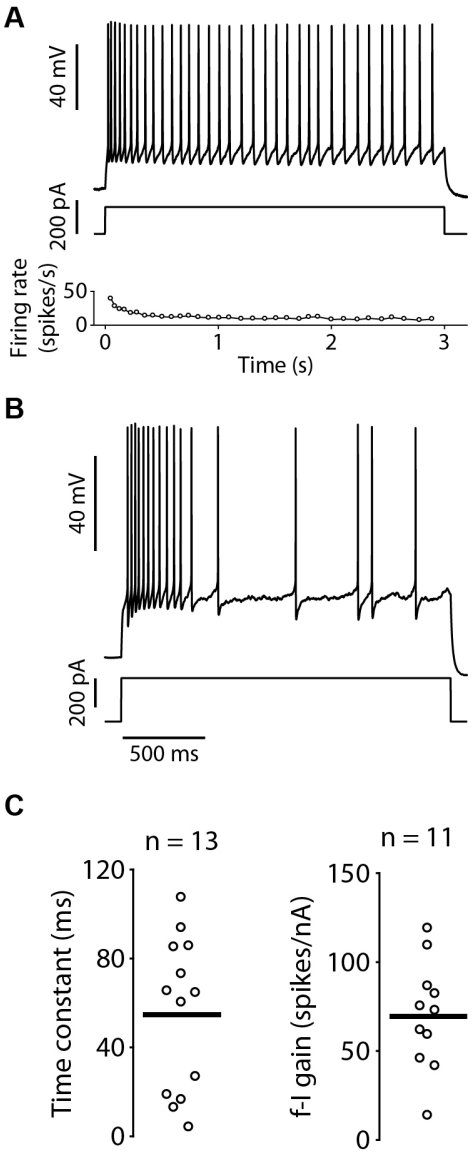


**Figure S5. Transplanted human ESC-derived neurons into the visual cortex show mature electrophysiological properties at 8-9 MPT. Related to Figure 6.**

(A) Sample membrane voltage traces of a cell showing a high accommodation index (only in 3 out of 11 cells in which APs were recorded), evoked by the intracellular injection of hyperpolarizing and depolarizing current steps. (B) Sample membrane voltage traces of a cell showing a typical interneuron-like discharge profile (only in 1 out of 11 cells recorded), evoked by the intracellular injection of hyperpolarizing and depolarizing current steps. (C) Single-cell passive (left) and active (right) membrane properties: open circles correspond to individual cells, with the bar representing the population mean. Both passive and active properties are in the ranges typically observed in cortical pyramidal neurons.

**Supplemental Experimental Procedures**

**Human pluripotent stem cell culture**

Experiments were performed using the H9 ESC line (Wicell) stably expressing GFP under the control of chicken β-actin promoter (H9-GFP line) generated previously (Espuny-Camacho et al., 2013). Human ESC were cultured and routinely passaged on mitotically inactivated mouse embryonic fibroblasts (MEFs), and routinely assayed for the expression of pluripotentcy markers, as previously described (Thomson, 1998).

**Human ESC differentiation into cortical progenitors and neural cells.**

Human ESC were differentiated towards cortical progenitors and neurons as previously described (Espuny-Camacho et al., 2013). In brief, human pluripotent stem cells were dissociated using Stem-Pro Accutase on day -2, (Invitrogen A11105) and plated on matrigel (BD, hES qualified matrigel) coated-coverslips/dishes at low confluency (5,000–10,000 cells/cm2) in MEF-conditioned hES/hiPS medium supplemented with ROCK inhibitor for cell survival (Y-27632; 10 μM Calbiochem, 688000). On day 0 of the differentiation, the medium was changed to "default differentiation medium" DDM supplemented with B27 (10 ml B27 per 500 ml DDM, GIBCO) for better human progenitor survival and with Noggin for neuroectoderm acquisition (100 ng/ml, R&D Systems). The medium was replenished every 2 days. After 16 DIV, noggin was withdrawn, and the medium was changed to DDM, supplemented with B27 (GIBCO), and changed every 2 days. At 24 DIV the human cortical progenitors were manually dissociated using a Pasteur cut pipette and a dilution of 100,000 cells per microliter was prepared for the animal transplantation experiments, as described in (Espuny-Camacho et al., 2013).

**Animal lesioning and grafting.**

All mouse experiments were performed with the approval of the Université Libre de Bruxelles Committee for animal welfare. Six- to 8-week-old adult NOD/SCID mice were anesthetized with ketamine and xylazine, followed by focal stereotactic injections of ibotenic acid to obtain focal cortical lesions performed either at the visual or motor cortex, as described before (Michelsen et al., 2015). In brief, the mice were placed in a stereotaxic frame, the dorsal surface of the head was shaved and a hole was drilled in the skull above the visual or motor cortex. 20 mg of ibotenic acid in 1μl distilled water was injected using a Hamilton syringe in the left visual (coordinates in mm B -3,1 / L - 2,4 / D 0,7) or left motor cortex (coordinates in mm B +1,2 / L 1,5 / D 0,8). The wound was closed and the mice left to recover in individual cages. Three days later, around 100.000 human ESC-derived cortical progenitors (in 0.5-1μl) were injected in the same coordinates, following the same procedure. The mice were again placed in individual cages for full recovery after surgery. A total number of 58 cases were analysed (n=37 for motor located transplants and n=21 for visual located transplants).

**Tissue preparation and immunofluorescence.**

For microscopy analysis, the mice were anesthetized with ketamine/xylazine and perfused with phosphate-buffered saline followed by 4% paraformaldehyde. The brain was removed and postfixed in the same fixative overnight and then cut in 75 μm slices on a Leica vibroslicer.

Immunofluorescence on grafted brains was performed as described previously (Espuny-Camacho et al., 2013). Briefly, sections were permeabilised and blocked for one hour at room temperature in solution containing 3% goat serum, 0.3% Triton X-100. The sections were then incubated overnight at 4 degrees with primary antibodies diluted in the same solution (for list of primary antibodies see table below). The following day PBS was used to wash the primary antibodies and the sections were incubated in the solution with secondary antibodies containing 3% goat serum, 0.3% Triton X-100 for 1 h at room temperature (for list of secondary antibodies see table below).

Antigen retrieval, when necessary, was performed by microwave boiling the slides in 10 mM tri-Sodium Citrate buffer pH 6.0 (VWR). Nuclei staining was performed using a specific anti-human nuclei antibody (see table below) or the pan-nuclear staining Hoechst.

Immunofluorescence images were acquired using a Zeiss LSM 510 META confocal microscope driven by ZEN 2009 software and 20x, 40x, 60x objectives and green, red, far-red and 2P lasers. Images were acquired as Z-series of stacks, 16-bit, 1024x1024 arrays that were consequently converted to maximum intensity projections (ImageJ). Image processing was performed with ImageJ and Adobe Photoshop/Illustrator (Adobe Systems) for preparation of multipanel Figures. Composite picture views were stitched manually from the individual confocal Z-series of stack images using Fiji and Adobe Photoshop.

| Primary antibodies | Species | Company | Catalog Number | Dilution |
|---|---|---|---|---|

| | | | | |
|---|---|---|---|---|
| beta III tubulin (Tuj1) | mouse | Covance | MMS-435P | 1/1000 |
| beta III tubulin | rabbit | Covance | PRB-435P | 1/1000 |
| beta III tubulin | chicken | Chemicon | AB9354 | 1/1000 |
| Brn2 | rabbit | Santa Cruz Biotech | Sc-6029 | 1/300 |
| Couptf1 | mouse | Abcam | Ab41858 | 1/500 |
| CTIP2 | rat | Abcam | ab18465-100 | 1/500 |
| Doublecortin | rabbit | Cell Signaling | | 1/500 |
| Foxg1 | rabbit | Abcam | ab18259 | 1/100 |
| Foxp2 | rabbit | Abcam | ab16046-100 | 1/5.000 |
| GFP | rabbit | Invitrogen | A6455 | 1/2000 |
| GFP | chicken | Abcam | AB13970-100 | 1/2000 |
| Homer1 | rabbit | Synaptic Systems | 160 003 | 1/1.000 |
| Human Nu antigen, clone 235-1 | mouse | Chemicon | MAB1281 | 1/500 |
| Human NCAM | mouse | Santa Cruz | ERIC 1 sc-106 | 1/500 |
| Ki67 | rabbit | Abcam | 833-500 | |
| MAP2 | mouse | Sigma | M1406-2ml | 1/2000 |
| Nestin | mouse | Covance | MMS-570P | 1/1000 |
| NeuN | mouse | Millipore | MAB377 | 1/300 |
| Pax6 | rabbit | Covance | PRB-278P | 1/2.500 |
| PH3 | rat | | | 1/1000 |
| Satb2 | rabbit | Abcam | ab34735 | 1/1000 |
| Synaptophysin | mouse | Synaptic Systems | 101 011 | 1/1.000 |
| Tau | rabbit | DAKO | 0024 | 1/500 |
| Tbr1 | rabbit | Gift from Hevner | | 1/10.000 |
| VGlut1 | rabbit | Synaptic Systems | 135 302 | 1/1000 |

| **Secondary antibodies** | **Species** | **Company** | **Dilution** |
|---|---|---|---|
| anti-mouse Alexa Fluor 488 | donkey | Invitrogen | 1/500 |
| anti-rabbit Alexa Fluor 488 | donkey | Invitrogen | 1/500 |
| anti-chicken Alexa Fluor 488 | chicken | Invitrogen | 1/500 |
| anti-mouse cyanin3 | donkey | Jackson Immunoresearch | 1/500 |
| anti-rabbit cyanin3 | donkey | Jackson Immunoresearch | 1/500 |
| anti-rat cyanin3 | donkey | Jackson Immunoresearch | 1/500 |
| anti-goat cyanin3 | donkey | Jackson Immunoresearch | 1/500 |
| anti-mouse cyanin5 | donkey | Jackson Immunoresearch | 1/500 |
| anti-rabbit cyanin5 | donkey | Jackson Immunoresearch | 1/500 |

**Quantification of axonal projections following grafting.**

Total number of GFP positive fibers and percentage of GFP positive fibers present at different cortical targets: striatum, thalamus and midbrain, were manually counted on coronal brain sections. GFP positive fibers were detected following immunofluorescence staining using GFP antibody, and were visualized using a Zeiss Axioplan upright fluorescence microscope equipped with 20x and 40x dry objectives.

For the striatum, the total number of fibers was counted in 1/6 of the sections collected for each individual brain. For the thalamus and midbrain, fibers were counted in 1/2 of the sections collected for each individual brain. Data are represented as mean ± s.e.m.. For the percentage of fibers, a total number of 10 and 8 animals were used for

quantification following transplantation into the visual and motor cortex, respectively. Statistical analyses were performed using the non-parametric Wilcoxon signed-rank test for paired data (to compare results in different brain areas in the same group of mice, either in visual or motor grafted mice), *p < 0.05, **p < 0.01. For the total number of fibers, 11 and 17 animals were used for quantification following transplantation into the visual and motor cortex, respectively. Statistical analyses were performed using the non-parametric Mann-Whitney test for unpaired data (to compare results in different groups of mice: visual versus motor grafted mice), *p < 0.05, **p < 0.01; ***p<0.001.

**Quantification of the graft bregma coordinates following transplantation into the visual and motor cortex.**
The bregma coordinates for the location of grafts following transplantation into the visual or motor cortex was analysed in coronal sections corresponding to 1/6 of the collected brain sections. Grafts were visualised by immunostaining using GFP antibody. The most rostral and the most caudal brain section containing the graft was analysed for bregma coordinates using the mouse brain atlas as a reference (Franklin and Paxinos, third edition 2007). Data are presented as mean bregma coordinates ± s.e.m., (n=7 visual grafts; n=4 motor grafts).

**Quantification of the percentage of Tbr1+ and Foxp2+ cells in motor and visual located transplants.**
The percentage of Tbr1 and Foxp2 positive cells detected among the total number of GFP and Hu Nuclei positive cells (human grafted cells) was determined on confocal acquired images using Fiji/ImageJ software from immunofluorescence stained brain sections. Confocal images were acquired using a Zeiss LSM 510 META microscope driven by ZEN 2009 software and 20x objective and green, red, far-red and 2P lasers. Images were acquired as Z-series of stacks of 5 μm step, 16-bit, 1024x1024 arrays that were consequently converted to maximum intensity projections and threshold adjusted using Default method to isolate specific Tbr1 and Foxp2 fluorescence (ImageJ). The percentage of Tbr1+ and Foxp2+ cells (number of cells over the total GFP+ HuNuclei+ counted) was quantified in 3 images blindly acquired from 2-3 different sections per animal. Data are represented as mean percentage ± s.e.m. (Tbr1 n=4 animals; 1.800-2.856 neurons; Foxp2 n=3-4 animals; 1.113-2.587 neurons). Statistical analysis was performed following Student's t test: n.s= non-significant.

**Quantification of the percentage of Couptf1+ cells in motor and visual located transplants.**
The percentage of Couptf1 positive cells detected among the total number of GFP positive cells (human grafted cells) was manually determined on confocal acquired images using Fiji/ImageJ software from immunofluorescence stained brain sections. Confocal images were acquired using a Zeiss LSM 510 META microscope driven by ZEN 2009 software and 40x objective and green, red, far-red and 2P lasers, using identical acquisition parameters as 16-bit, 1024x1024 arrays. Z-series stacks were then converted in ImageJ to maximum intensity projections and threshold adjusted using Triangle method to isolate specific Couptf1 fluorescence. The percentage of Couptf1+ cells (number of cells over the total GFP+ counted) was quantified in 4 different areas blindly set in all images. Data are represented as mean percentage ± s.e.m. (n=3 animals; 1.400-2.116 neurons). Statistical analysis was performed following Student's t test: *p < 0.05.

**Quantification of the graft volume in motor and visual located transplants**
The graft volume was measured from confocal acquired images from the graft in serial coronal sections corresponding to a sixth of the mouse brain. Mouse brain sections were immunostained with GFP antibody and confocal images were acquired using a Zeiss LSM 510 META microscope driven by ZEN 2009 software with a 10x objective using identical acquisition parameters as 16-bit. Z-series stacks of 10 μm step were acquired for a total of 6 steps (60 μm thickness). The volume of the graft contained within one individual section was calculated using Fiji/plugin software, and the total graft volume corresponding to 1/6 of the brain was determined by adding the individual volumes of each of the sections with a graft. Data are represented as mean percentage ± s.e.m. (n=8 animals grafted into the visual cortex; n=8 animals grafted into the motor cortex). Statistical analysis was performed following Student's t test: n.s= non-significant.

**Quantification of the proportion of transplants with subcortical projections**
We quantified the proportion of visual and motor located transplants projecting GFP positive fibers into the striatum, thalamus and midbrain over the total number of visual and motor transplanted animals. Quantification was performed by manual counting of the axonal projections in immunofluorescence stained brain sections using the GFP antibody. Images were acquired using a Zeiss Axioplan upright confocal microscope equipped with 20x and 40x dry objectives.
For the quantification of the proportion of animals with fibers present in the striatum, we quantified 1/6 of the sections collected for each individual brain. For the quantification of the proportion of animals with fibers in thalamus and midbrain, 1/2 of the sections collected for each individual brain were analysed. Data are represented as mean percentage ± s.e.p. (visual grafts: n=11 animals; motor grafts: n=17 animals). Statistical analysis was performed following Z test for proportions: ns= non-significant; *p < 0.05.

***Ex vivo* electrophysiology**
Electrophysiological recordings were performed on grafted neurons in acute brain slices from mice at 8 and 9 months post-transplantation. Acute brain slices were obtained as follows: Mice were deeply anesthetized with a mixture of

ketamine and xylazine, and transcardially perfused with ice-cold solution containing (in mM) 80 NaCl, 2.5 KCl, 1.25 $NaH_2PO_4$, 1 $CaCl_2$, 5 $MgCl_2$, 30 $NaHCO_3$, 25 D-glucose and 75 sucrose (gassed with 95% $O_2$/5% $CO_2$). The brain was rapidly removed, trimmed by cutting off cerebellum and hindbrain directly behind the occipital cortex, and glued to the stage of a VT1000-S vibratome (Leica Instruments, Nussloch, Germany) to cut 300 m thick coronal slices in the same solution at 4 °C. Slices were incubated after cutting in artificial CSF (aCSF) containing (in mM) 125 NaCl, 2.5 KCl, 1.25 $NaH_2PO_4$, 2 $CaCl_2$, 1 $MgCl_2$, 30 $NaHCO_3$ and 25 D-glucose (gassed with 95% $O_2$/5% $CO_2$) for at least 20 minutes and stored thereafter at room temperature for up to 7 h. For recording one slice at a time was transferred to a chamber and continuously perfused with aCSF at 1.5 ml/min. Transplanted cells were identified by their EGFP fluorescence and visualized using an upright microscope equipped with infrared differential interference contrast (Leica Microsystems, DMLFS, Belgium). Recordings were performed at 33 ± 1 °C. For recordings, patch pipettes (resistance 6–9 M containing (in mM): 115 K-gluconate, 20 KCl, 10 HEPES, 4 Mg-ATP, 0.3 $Na_2$-GTP, 10 $Na_2$-phosphocreatine, pH adjusted to 7.3 with KOH. Current clamp recordings were performed with an EPC 10 patch clamp amplifier (HEKA Electronics, Lambrecht/Pfalz, Germany): neither bridge balance nor capacitance compensation were used online: rather, electrode kernels were estimated throughout the experiment by following the procedure described in (Brette et al., 2008) and subsequently used to compensate offline the recorded data. Liquid junction potentials were left uncorrected. Signals were recorded at a rate of 20 kHz. All electrophysiological recordings were analyzed using MATLAB (The Mathworks, Natick, MA). To deliver bipolar extracellular electrical stimuli and elicit compound synaptic responses, we used an ISO-Flex stimulus isolator (AMPI, Israel) connected to two platinum wires inserted in a theta-glass pipette (1401021, Hilgenberg, Malsfeld, Germany) filled with aCSF. This electrode was placed at distances between 100 and 400 μm from the recorded neuron and current-controlled stimuli had amplitude in the range 100-1000 μA and duration of 100 μs. In some experiments, synaptic inputs were blocked by adding to the bath selective antagonists of ligand-gated channels (i.e., AP-V, 50 μM; CNQX, 20 μM; GABAzine, 10 μM). All the chemicals were from Sigma, Belgium.

**Accommodation index**

In order to quantify the degree of spike frequency adaptation, the accommodation index $A$ was computed according to (Druckmann et al., 2007) as

$$A = \left(N_{spks} - 4 - 1\right)^{-1} \cdot \sum_{q=4}^{N_{spks}-1} \left(\mathrm{ISI}_q - \mathrm{ISI}_{q-1}\right) / \left(\mathrm{ISI}_q + \mathrm{ISI}_{q-1}\right) \tag{6}$$

where $N_{spks}$ is the number of spikes evoked by a constant depolarizing step of current, $\mathrm{ISI}_q$ is the $q$-th inter-spike interval, and where the first four spikes were always discarded from the analysis, to ensure that the firing discharge had reached a steady-state regime.

**Supplemental References**


Brette, R., Piwkowska, Z., Monier, C., Rudolph-Lilith, M., Fournier, J., Levy, M., . . . Destexhe, A. (2008). High-resolution intracellular recordings using a real-time computational model of the electrode. *Neuron, 59*(3), 379-391. doi:10.1016/j.neuron.2008.06.021

Druckmann, S., Banitt, Y., Gidon, A., Schürmann, F., Markram, H., and Segev, I. (2007). A novel multiple objective optimization framework for constraining conductance-based neuron models by experimental data. Front. Neurosci. *1*, 7–18.

Franklin, K.B.J. and Paxinos, G., (Third edition 2007). The mouse brain in stereotaxic coordinates. Academic Press.

Thomson, J.A. (1998). Embryonic Stem Cell Lines Derived from Human Blastocysts. Science (80-. ). *282*, 1145–1147.